American Mineralogist, Volume 96, pages 521–533, 2011

Critical evaluation of the revised akdalaite model for ferrihydrite

A. Manceau*

ISTerre-Maison des Géosciences, CNRS and Université J. Fourier, BP 53, 38041 Grenoble, France

Abstract

The defect-free akdalaite model (fhyd6) for six-line ferrihydrite (6Fh) derived from a pair distribution function (PDF) analysis of high-energy X-ray scattering (HEXS) data was revised (model ferrifh) by Michel et al (2010) using data from a sample produced by heating two-line ferrihydrite (2Fh) at 175 °C for 8 h in the presence of citrate. We show here that the scattering pattern for this sample is similar if not the same as that for hydromaghemite, which in turn is a mixture of maghemite (γ-Fe_2O_3), hematite and 6Fh. As in the case of fhyd6, the PDF of ferrifh was regressed using the structure of the weakly hydrated phase akdalaite [$Al_{10}O_{14}(OH)_2$] after substituting Fe for Al as a starting model. We show that the ferrifh model is implausible for the following reasons. (1) It is derived from a sample, ferrifh, that appears to be hydromaghemite, not pure 6Fh. (2) It has 20% tetrahedral Fe, a coordination that had been eliminated previously using XANES, Mössbauer, and EELS spectroscopies. (3) 75% of the Fe octahedra have shared edge lengths considerably longer than the shortest unshared edges in violation of Pauling's distortion rule. (4) Three tetrahedral Fe-O bonds are longer than three octahedral Fe-O bonds, inducing significant polyhedral distortions. And (5) the calculated composition [$Fe_{10}O_{14}(OH)_2 \cdot 1.2H_2O$] disagrees with literature data on weight loss from dehydration for 6Fh.

We present an alternative interpretation of the histogram of Fe-Fe distances up to 3.7 Å obtained from the PDF of the fhyd6 ferrihydrite as a mixture of local structures of goethite/akaganeite (α/β-FeOOH) and feroxyhite/hematite (δ-FeOOH/α-Fe_2O_3). Within this interpretation Fe only occupies octahedra that are bonded to each other by faces, edges, or double-corners. This polyhedral connectivity is confirmed experimentally by analysis of the EXAFS spectra of six-line ferrihydrites measured at room and liquid helium temperature. The Fe-Fe pairs from EXAFS data are described reasonably well by a mixture of approximately 70% feroxyhite (containing some nanohematite) and 30% akaganeite, without resorting to other phases. This set of evidence indicates that HEXS data are consistent with the Drits model for ferrihydrite (Drits et al. 1993a).

Keywords: Ferrihydrite, diffraction, HEXS, PDF, EXAFS, structure, oxyhydroxide, nanoparticle

Introduction

Ferrihydrite (Fh) is a widespread poorly crystallized hydrous ferric oxyhydroxide at the Earth's surface (Jambor and Dutrizac 1998; Cornell and Schwertmann 2003) and a likely constituent in extraterrestrial materials (Fortin and Langley 2005; Farrand et al. 2009). In the laboratory, it is formed typically by the rapid neutralization of a ferric nitrate solution (Flynn 1984). Fresh precipitates contain only two broad X-ray diffraction (XRD) bands if the hydrolysis is performed at room temperature and a maximum of six strong lines if the ferric solution is heated to about 80 °C (Towe and Bradley 1967). The principal difference between these two diffraction end-members is the size of the constitutive crystallites (Combes et al. 1989, 1990; Drits et al. 1993a; Manceau and Drits 1993). Numerical simulations of homogenous precipitation with fast nucleation rates suggest that Fh is a mixture of nanoparticles with different metastable structures and can never be a single phase (Marchand and Rancourt 2009). The coexistence of different structures, predicted for nucleation in the highly supersaturated conditions at which Fh is synthesized, is consistent with the structural model established by X-ray diffraction (Drits et al. 1993a) that describes Fh as a mixture of two principal components, named f- and d-phases (Fig. 1), with minor nanohematite (α-Fe_2O_3). This model is hereafter referred to as Drits model.

The f-phase is a defect-free double-hexagonal ABAC stacking of close-packed oxygen and hydroxyls (space group $P\bar{3}1c$). The Fe atoms are randomly distributed over octahedral sites having an occupancy probability of 0.5, and displaced in the direction of the B and C anionic planes. This displacement suggests that: (1) the hexagonal ABA and ACA domains have no, or few, shared faces; (2) the B and C planes contain mainly O atoms (occ. = 0.85); and (3) the A planes contain mainly hydroxyls (occ. = 1) to satisfy electrostatic requirements. The d-phase is defective and modeled by random sequences of enantiomorphous ABA and ACA layers. The Fe octahedra share faces within each layer and the Fe-Fe pairs have a high degree of local ordering in and perpendicular to the anionic planes similar to feroxyhite (δ-FeOOH; Drits et al. 1993b). Individual crystallites and their coherently diffracting domains have a spherical or polyhedral habit (Supplementary Fig. 1[1]; Cowley et al. 2000; Pan et al. 2009).

* E-mail: manceau@ujf-grenoble.fr

[1] Deposit item AM-11-015, Supplementary materials, tables, and figures. Deposit items are available two ways: For a paper copy contact the Business Office of the Mineralogical Society of America (see inside front cover of recent issue) for price information. For an electronic copy visit the MSA web site at http://www.minsocam.org, go to the *American Mineralogist* Contents, find the table of contents for the specific volume/issue wanted, and then click on the deposit link there.

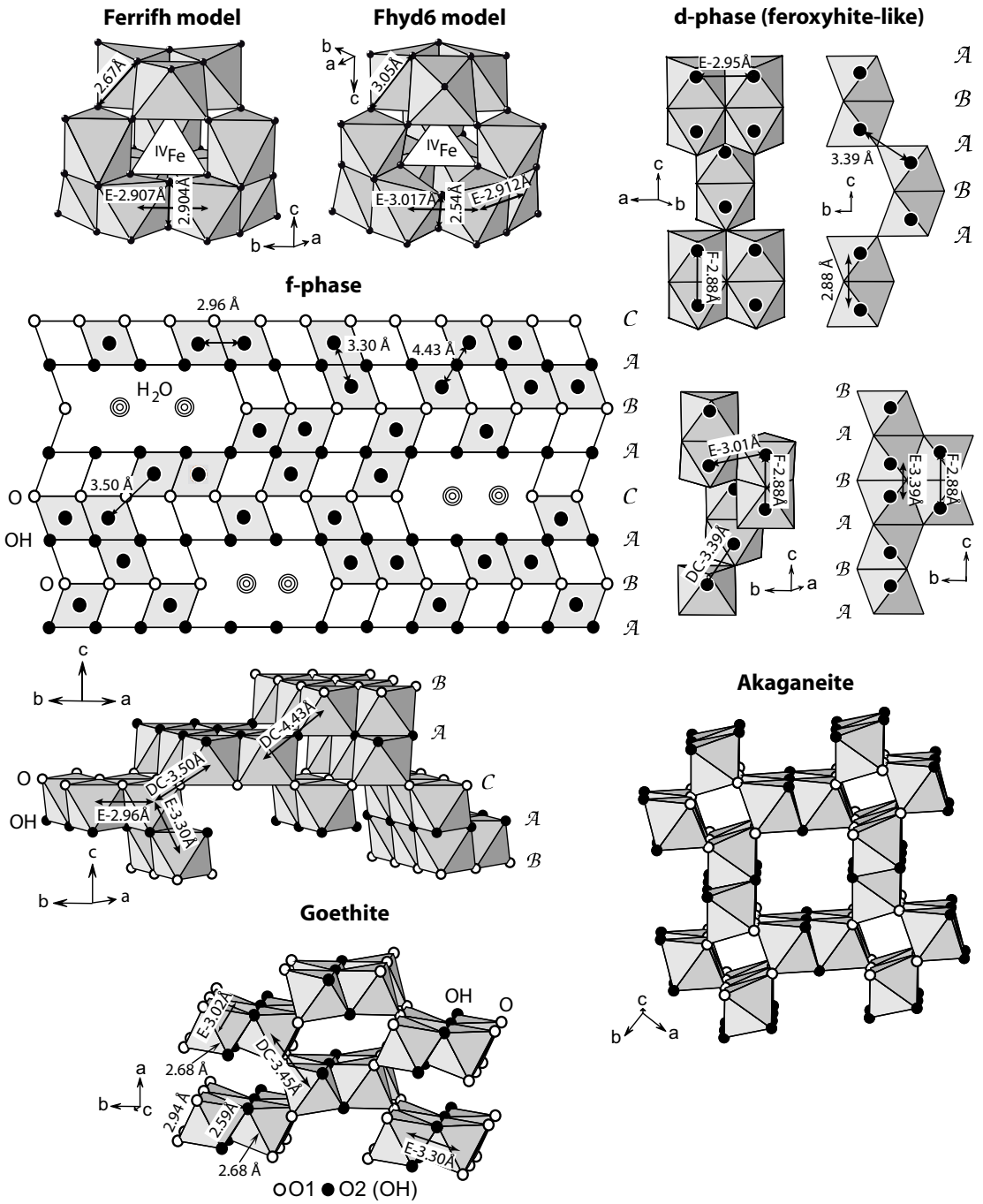

FIGURE 1. Structural representation of the two akdalaite-like models (ferrifh and fhyd6), the f- and d-phases (defective feroxyhite) of the Drits model, goethite and akaganeite. The f-phase is represented in projection along the [$\bar{1}\bar{1}$0] axis and in perspective to show the goethite- and akaganeite-like polyhedral associations. The two polyhedral depictions of the d-phase are from Figures 6 (top) and 8 (bottom) of Drits et al. (1993b).

The f- and d-phases were confirmed by neutron diffraction (Jansen et al. 2002), and all three components have been observed using high-resolution transmission electron microscopy (HR-TEM), including single-crystal electron nanodiffraction (Janney et al. 2000, 2001; Cowley et al. 2000). The feroxyhite-type local structure of the d-phase was described in terms of a "double-chain structure" by Janney et al. (2000), but in reality the two structural components are the same (Manceau 2009). Maghemite (γ-Fe_2O_3), magnetite (Fe_3O_4), and even wüstite (FeO) grains also were observed by TEM, but are essentially artifacts produced by the migration of Fe atoms from octahedral to tetrahedral sites and the reduction of Fe^{3+} to Fe^{2+} induced by exposure to the electron beam (Drits et al. 1995; Pan et al. 2006, 2009, 2010).

An alternative model, named fhyd6, was derived from the pair distribution function (PDF) analysis of high-energy X-ray scattering (HEXS) data (Fig. 1; Michel et al. 2007). The new model is single-phase and isostructural with the mineral akdalaite [$Al_{10}O_{14}(OH)_2$] and its synthetic isomorph tohdite, a crystalline

and essentially anhydrous aluminum hydroxide compound consisting of a periodic assemblage of Baker-Figgis δ-Keggin isomers (i.e., Al_{13} entities; Yamaguchi et al. 1964; Yamaguchi and Okumiya 1969; Hwang et al. 2006). The anionic packing is also ABAC and the hydroxyls are also on the A planes, but three-fourth of the A positions are occupied by O atoms and 20% of the Fe atoms are tetrahedral. Akdalaite has a similar local coordination environment to maghemite (γ-Fe_2O_3), a ferrimagnetic spinel ferrite where each oxygen of an Fe tetrahedron is shared by three edge-sharing Fe octahedra, and which has no shared polyhedral faces.

The fhyd6 model has been challenged by four groups using different and complementary arguments (Rancourt and Meunier 2008; Hiemstra and van Riemsdijk 2009; Manceau 2009; Pan et al. 2010). The main criticisms were the following. (1) The fhyd6 model is completely periodic (i.e., defect-free), does not describe X-ray diffraction and EXAFS spectroscopic data, and is inconsistent with electron microscopy, XANES, Mössbauer, and EELS results. (2) Bond-valence calculation shows that it has 20% tetravalent octahedral iron ($^{VI}Fe^{4+}$), 20% divalent tetrahedral iron ($^{IV}Fe^{2+}$), and some ^{IV}Fe-O distances equal to or larger than the $^{VI}Fe^{3+}$-O distances, thus violating Pauling's 2nd rule. (3) It is anomalously H-poor for a hydrous oxyhydroxide formed at the surface of the earth. And (4) its molar mass is unrealistically close to that of hematite (M = 82 g/mol Fe vs. 81 g/mol Fe) and its mass density is significantly higher than experimental and calculated values (ρ = 4.8–4.9 g/cm^3 vs. 3.96 and 4.15 ± 0.1 g/cm^3).

More recently, Michel et al. (2010) proposed a new akdalaite-like structural model, named ferrifh, as a replacement of the former fhyd6 model (Michel et al. 2007). Ferrifh was formed by heating a two-line ferrihydrite (named fh) at 175 °C for 8 h in the presence of citrate, a protocol followed usually to synthesize hydromaghemite (Barron et al. 2003; Liu et al. 2008). This synthesis procedure differs from the ferric salt hydrolysis route at ~80 °C where no organic molecule is used. This latter hydrolysis route is generally used to synthesize 6Fh (Towe and Bradley 1967), and was followed previously to synthesize the sample from which the fhyd6 model was derived. The ferrifh and fhyd6 models share however the same basic polyhedral structure of akdalaite, have a low density of defects, and all O and Fe sites are fully occupied (occ. = 1). Therefore, ferrifh also has 20% tetrahedral Fe (^{IV}Fe) and no shared octahedral faces, in contrast to the Drits model (Drits et al. 1993a). The two akdalaite models mainly differ from each other in the positions of Fe and O atoms in the unit cell, where the coordinates of ferrifh better satisfy Pauling's second rule. The ferrifh model was considered general by the authors because it described equally well the PDFs of the initial two-line ferrihydrite sample (fh) and the heated sample (ferrifh). The fh and ferrifh samples differ mainly in terms of particle size, structural relaxation (i.e., unit-cell parameters), and the presence in fh of defects in the form of cation vacancies filled with protons as hydroxyls to balance the total charge. Between 45 and 50% of the tetrahedral sites are empty in fh, whereas they are all occupied in ferrifh (occ. = 1), which implies that the amount of tetrahedral Fe in ferrihydrite increases from approximately 10 to 20% in going from two-line to six-line ferrihydrite.

This article has two main objectives. The first is to discuss the new ferrifh model, which is problematic with respect to fundamental crystal-chemical rules similarly to the previous fhyd6 model.

The second objective is to examine and discuss the Fe-Fe distances obtained by PDF and EXAFS spectroscopy from the perspective of the Drits model (Drits et al. 1993a). Interatomic distances from the PDF of fhyd6 reveals good agreement with EXAFS data of 6Fh, and shows that this mineral can be described as a simple assemblage of akaganeite-type (β-FeOOH) and feroxyhite-type (δ-FeOOH) polyhedral structures at the local scale. This result is consistent with the Drits model, which excludes tetrahedral coordination and includes the sharing of faces (F), edges (E), and double corners (DC) among Fe octahedra.

Ferrifh is hydromaghemite, not ferrihydrite

The XRD pattern of ferrifh is the same as that of hydromaghemite and differs from the pattern of six-line ferrihydrite by the presence of a double peak at 1.60–1.64 Å (Fig. 2). The absence of this peak in 6Fh is not a particle shape effect because the diffracting nano-crystallites of 6Fh are rounded and their domain size is isometric (Supplementary Fig. 1[1]). Hydromaghemite has been described previously and named in analogy to hydrohematite (Barron et al. 2003; Liu et al. 2008). However, this compound is not a pure phase because, according to XRD, it is a mixture of 6Fh, hematite, residual 2Fh, and low tetrahedral maghemite (γ-Fe_2O_3; de Boer and Dekkers 2001).

Two-line ferrihydrite (2Fh) converts directly to hematite upon heating, but evolves partially toward an intermediate spinel phase (i.e., maghemite) in the presence of organic reductants, such as citrate (Campbell et al. 1997). In contrast to 2Fh, 6Fh always transforms directly to hematite (Mazzetti and Thistlethwaite 2002; Barron et al. 2003). The formation of spinel from 2Fh is considered to proceed by partial reduction of ferric iron followed by partial (magnetite, Fe_3O_4) or total (maghemite) reoxidation depending on oxygen availability. As the formation of spinel requires the reduction of ferric iron, and thus a reductant such as a carbon source, this intermediate ^{IV}Fe-containing phase in the transformation of 2Fh into hematite cannot be used as evidence of the existence of tetrahedral Fe in 2Fh (Campbell et al. 1997). Maghemite contains approximately 20 to 37% ^{IV}Fe (Greaves 1983; Shmakov et al. 1995; Corrias et al. 2000), and hydromaghemite less because it is a mixture of ^{IV}Fe-free (i.e., hematite, Fh) and ^{IV}Fe-depleted (i.e., low-tetrahedral maghemite) (oxyhydr)oxides (Liu et al. 2008). The hydromaghemite nature of the ferrifh sample is consistent with its pronounced ferrimagnetism as maghemite is ferrimagnetic and six-line ferrihydrite antiferromagnetic (Pankhurst and Pollard 1992; Guyodo et al. 2006). Thus, the revised akdalaite model was established on a material that is a phase mixture and contains ^{IV}Fe in another constituent (maghemite) than 6Fh.

Non-uniqueness of PDF models for defective minerals

The HEXS data from Michel et al. (2010) were recorded on a series of two-line ferrihydrites heated at 175 °C for 0 to 14 h. The 2Fh component dominated in the first few hours (sample fh), hydromaghemite (ferrifh) at 8 h, and hematite after 12 h. Thus, the PDFs from the heated samples represented a mixture of at least three compounds: two-line ferrihydrite, hydromaghemite, and hematite. Michel et al. (2010) extracted PDFs for each of the three materials using multivariate curve resolution (MCR) analysis (de Juan and Tauler 2003), which is similar to principal

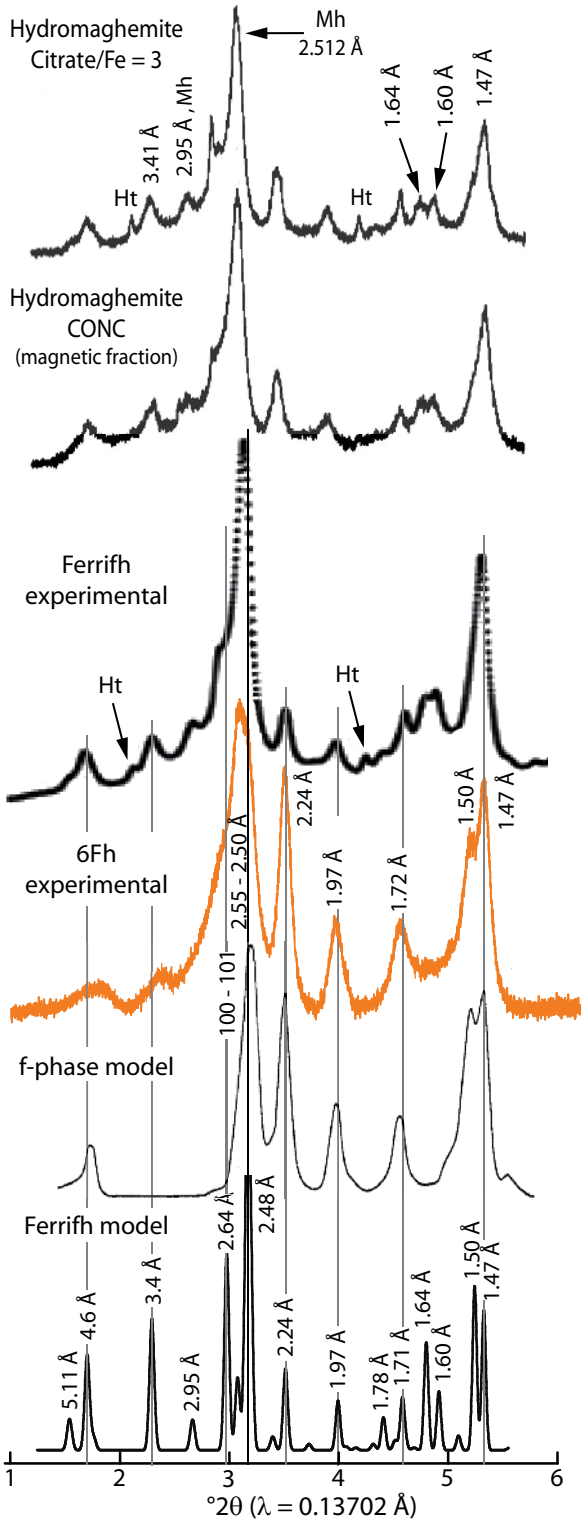

FIGURE 2. Experimental X-ray diffraction patterns for hydromaghemite (Barron et al. 2003), ferrifh (Michel et al. 2010), and six-line ferrihydrite (6Fh from Manceau 2009), and calculated patterns for the f-phase (Drits et al. 1993a) and ferrifh. CONC is the magnetic fraction of the citrate/Fe = 3 hydromaghemite (Barron et al. 2003). From the position and symmetry of the 2.50–2.55 Å line, the 6Fh sample has a higher proportion of the d-phase than the 6-Fh sample modeled by Drits et al. (1993a). See also Figure 7.

component analysis (Malinowski 1991; Manceau et al. 2002) in that individual PDFs are mathematically independent (i.e., their eigenvectors are orthogonal). Consequently, the PDFs of fh and hydromaghemite cannot be reproduced theoretically with the same structural model (ferrifh). A single model that can explain data from at least two different materials (2Fh/6Fh and hydromaghemite), the last one being a mixture of three phases (2Fh/6Fh, maghemite, hematite; Barron et al. 2003; Liu et al. 2008), indicates that the data were overfit. The derivation of two akdalaite-like structures, both violating Pauling's rules, suggests that PDF does not contain enough information to uniquely determine crystallographic models for defective minerals (Juhas et al. 2006), and that independent scientific and statistical constraints on parameters are required to obtain meaningful parameter values from HEXS measurements. In fact, the PDFfit2 (PDFgui) User Guide provides a warning against the non-uniqueness of solutions for nanocrystalline materials (Farrow et al. 2007; Manceau 2010). A similar cautionary note was made by Fernandez-Martinez et al. (2010) on their PDF study of schwertmannite, another defective Fe oxyhydroxide. These authors also concluded that information about the long-range order of defective minerals is more reliably extracted from the quantitative analysis of powder diffraction data than PDF.

Crystal-chemical irregularities of the revised akdalaite model

The unbalance of electrical charges, which was a major shortcoming of the fhyd6 model, has been addressed in the revised (i.e., ferrifh) model. However, a new problem has emerged, which is the violation of Pauling's distortion rule (1929) combined with the presence of unusually short Fe_E-Fe_E distances of 2.907 Å. The cation-cation Coulombic repulsive force, which increases quadratically when two polyhedra are brought closer together by the sharing of an edge (E) or a face (F), is shielded in ionic structures by the shortening of shared (sh) edges and the compensatory lengthening of unshared (unsh) edges. In hematite, $d(O_{sh}\text{-}O_{sh})$ = 2.67 Å and $d(O_{unsh}\text{-}O_{unsh})$ = 2.89–3.03 Å for a face-sharing Fe separation of $d(Fe_F\text{-}Fe_F)$ = 2.90 Å (Blake et al. 1966). In goethite (α-FeOOH), the edge lengths and Fe-Fe separations are $d(OH_{sh}\text{-}OH_{sh})$ = 2.59 Å, $d(Fe_E\text{-}Fe_E)$ = 3.30 Å; $d(O_{sh}\text{-}OH_{sh})$ = 2.68 Å, $d(Fe_E\text{-}Fe_E)$ = 3.02 Å; and $d(O_{unsh}\text{-}O_{unsh})$ = 2.90–3.02 Å (Hazemann et al. 1991). In tohdite, the akdalaite model structure used to simulate HEXS data, $d(O_{sh}\text{-}OH_{sh})$ = 2.63 Å and $d(O_{unsh}\text{-}O_{unsh})$ = 2.72 Å (Yamaguchi and Okumiya 1969), all in agreement with Pauling's distortion rule (Fig. 1).

In contrast, the ferrifh model has shared edge lengths [$d(O_{sh}\text{-}OH_{sh})$ = 2.904 Å] considerably longer than the shortest unshared edges [$d(O_{unsh}\text{-}O_{unsh})$ = 2.67 Å], in violation of the distortion rule. It also produces unrealistically short Fe_E-Fe_E distances of 2.907 Å across the long shared edges (Fig. 1). The model Fe_E-Fe_E distance provides indirect evidence for face-sharing octahedra because the shortest Fe_E-Fe_E distance observed in ferric oxyhydroxides is that of 3.02 Å in goethite (Hazemann et al. 1991). In the Drits model, this short Fe-Fe distance is observed and attributed to the sharing of faces between Fe-Fe octahedral pairs from the d-phase (Fig. 1). In addition to the questionable structural assignment of these O-O and Fe-Fe pair correlations seen in the reported PDFs derived from the HEXS data, the improbability of the ferrifh model is further supported by the presence of longer tetrahedral

Fe-O distances than the octahedral Fe-O (i.e., 1.932 vs. 1.882). This is in contrast to the Fe-O distances observed in maghemite: ^{IV}Fe-O = 1.85 ± 0.02 Å vs. ^{VI}Fe-O = 2.05 ± 0.03 Å and 2.11 ± 0.01 Å (Shmakov et al. 1995).

Pauling's deformation rule can be violated, however, in severely distorted materials, such as the transition alumina κ-Al_2O_3 (Ollivier et al. 1997) and the low-chlorine akaganeite (Takagi et al. 2010). In low-Cl akaganeite, some O_{unsh}-O_{unsh} pairs are closer together (2.54 Å) than O_{sh}-O_{sh} pairs (3.21 Å). However, the Fe_E-Fe_E distances across the long edges are 3.29 Å, compared to 2.90 Å in the ferrifh model, and the shortest Fe_E-Fe_E distance in this akaganeite is 3.03 Å, similar to goethite. Therefore, what is really atypical in the ferrifh model is the combination of two crystal-chemical irregularities: the elongation of shared edges and the extreme shortening of the Fe-Fe distances across these shared edges. If, for whatever reason, one shared edge is elongated beyond normal, then for electrostatic reasons the two cations from the shared octahedra should move apart, not get closer to each other. In addition, EXAFS results presented below suggest that the $Fe(O,OH)_6$ octahedra are less distorted in 6Fh than in low-Cl akaganeite.

In summary, the revised akdalaite model of ferrihydrite is structurally and chemically implausible for the following reasons. (1) It is derived from a sample, ferrifh, which is hydromaghemite, not a six-line ferrihydrite. (2) It has 20% tetrahedral Fe. (3) 75% of the Fe octahedra have shared oxygen edges longer than unshared edges, and three tetrahedral Fe-O distances are longer (1.932 Å) than three octahedral distances (1.882 Å). (4) The short correlation at 2.907 Å attributed to two Fe atoms across the abnormally long O_{sh}-OH_{sh} shared edge of 2.904 Å is more typical of a shared face, not a shared edge. And (5) ferrifh has a calculated composition [$Fe_{10}O_{14}(OH)_2 \cdot 1.2H_2O$] in disagreement with the measured weight loss from dehydration for six-line ferrihydrite equal to 5–12% at temperatures <100–120 °C and to 10.5–15% from 100–120 °C to 800–1000 °C (Saleh and Jones 1984; Eggleton and Fitzpatrick 1988). There is no natural mineral at the surface of the Earth that is as hydrated, but contains as little structural hydroxyl and water. Supporting evidence for the occurrence of shared faces in 6Fh is provided below from polyhedral considerations and by EXAFS spectroscopy.

Polyhedral connectivity

PDF is not an ab initio technique and the regression algorithm finds the best solution that it can, which is normally highly dependent on the starting structure (e.g., akdalaite), but consistent with data. Since the PDF maxima were well reproduced in the fhyd6 and ferrifh model-fits, despite the implausibility of the refined akdalaite structures, it is possible that the fitting software had enough flexibility to converge nonetheless to the correct values of the dominant correlations in these two mineralogically distinct materials. In other words, having the wrong starting model does not necessarily imply that all regressed PDF pairs are at the wrong distances. If the fit is good, then the most abundant correlations may be at the right position, but the 3D representation of the structure using the space-group symmetries and lattice parameters of the model will be incorrect, as indicated for example by the violation of crystal-chemical rules. The objective of this section is to show that the Fe-Fe PDF correlations for ferrihydrite are actually consistent with the Drits model, which excludes tetrahedral coordination and includes the sharing of faces (F), edges (E), and double corners (DC) among Fe octahedra.

The way octahedra are linked together in ferrihydrite may be inferred from the histograms of the Fe-Fe distances obtained by PDF using a polyhedral approach (Manceau and Combes 1988; Manceau and Drits 1993). Based on the structures of ferric (oxyhydrox)oxides, a shared face gives a Fe-Fe distance of 2.88–2.90 Å (feroxyhite, hematite), and a shared edge gives a Fe-Fe distance of ~2.97 Å when formed by two O^{2-} (α-Fe_2O_3), 3.02–3.03 Å when formed by one O^{2-} and one OH^- (α/β-FeOOH), and 3.30–3.35 Å when formed by two OH^- (α/β-FeOOH) (Figs. 1 and 3a–3c). Octahedra that are linked by double-corners (DCs) have Fe-Fe separations of 3.36 Å in hematite and 3.45–3.52 Å in goethite and akaganeite. The atomic coordinates of feroxyhite are not known precisely because this phase has a defective structure, similarly to the d-phase (Drits et al. 1993b). Lepidocrocite (γ-FeOOH) is not considered because it has only O_{sh}-O_{sh} edges (Fig. 3b) and its octahedral chains are not cross-linked in contrast to α/β-FeOOH. Therefore, it has single-corner sharing octahedra (C) instead of DC and an Fe-Fe separation of 3.87 Å (Zhukhlistov 2001), a correlation not observed in the PDF for ferrihydrite.

The histogram of the Fe-Fe distances for the fhyd6 sample, which is a nominal six-line ferrihydrite (6Fh), can be described in the 2.90–3.6 Å interval using the histograms of α/β-FeOOH and δ-FeOOH/α-Fe_2O_3 (Fig. 3). Accordingly, three types of octahedral linkages may be prominent: F, E, and DC, in agreement with the Drits model. In contrast, the akdalaite model has no shared faces, and 12 shared corners between tetrahedra and octahedra [i.e., each of the four $^{IV}FeO_4$ apices is connected to three $^{VI}Fe(O,OH)_6$] (Fig. 1). The short Fe-Fe distance of 2.912 Å in the PDF of fhyd6 attributed in the akdalaite model to an edge linkage is more likely from a face linkage. The origin of the recurrent structural irregularities in the fhyd6 and ferrifh models likely resides, among other factors, in the fact that shared face does not exist in akdalaite, while this prescribed structure contains 20% tetrahedral Fe, which is non-existent in ferrihydrite (fhyd6 sample) and minor in hydromaghemite (ferrifh sample).

The intense pair correlation at about 3.4–3.5 Å in the PDF of fhyd6 was interpreted as supporting evidence for the presence of ^{IV}Fe (Parise et al. 2010; Xu et al. 2011). This interpretation is realistic because corner-linked (C) $^{IV}FeO_4$-$^{VI}Fe(O,OH)_6$ polyhedra in maghemite and [Fe_{13}] α-Keggin cluster (Bino et al. 2002) have this distance. However, it is observed also for ^{VI}Fe-^{VI}Fe DC bridging in α/β-FeOOH (Fig. 1). Thus, this Fe-Fe correlation does not allow differentiation between the akdalaite and the Drits models.

Evidence for face-sharing octahedra in ferrihydrite from EXAFS

The resolution in distance of EXAFS spectroscopy at the Fe K-edge is at best $\Delta R = \pi/2k_{max} = 0.11$ Å for $k_{max} = 14$ Å^{-1} and 0.09 Å for $k_{max} = 17$ Å^{-1}, and therefore sufficient to separate the Fe_E-Fe_E and Fe_F-Fe_F pairs in feroxyhite ($\Delta R = 3.01 - 2.88 = 0.13$ Å) but not in hematite ($\Delta R = 2.97 - 2.90 = 0.07$ Å; Figs. 1 and 3a). The distance resolution of PDF is not better than EXAFS, at least for nanocrystalline materials, because $Q_{max} = 28$ Å^{-1} in the study by Michel et al. (2010), and Q_{max}(PDF) = 2 × k_{max}(EXAFS)

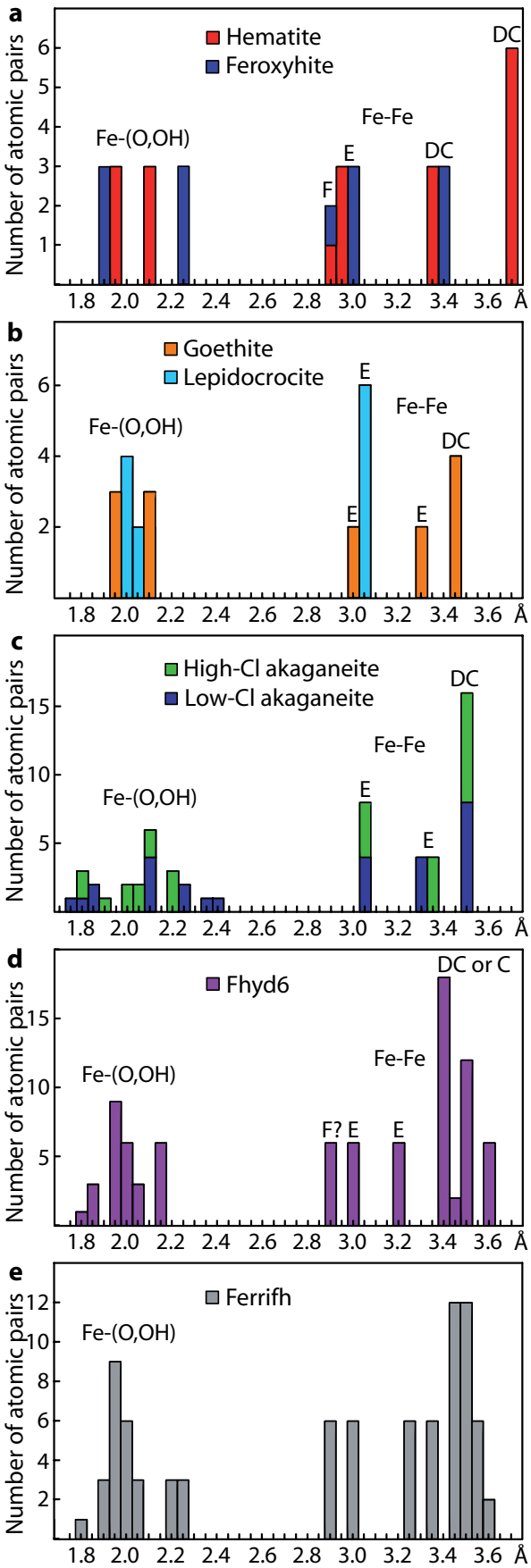

for the same distance resolution. The separation of the two Fe pairs is also complicated in the PDF technique by the composite nature of the second $G(r)$ peak at $r = 3$ Å (equivalent to the radial distribution function in EXAFS, Fig. 4), which includes not only the Fe_F-Fe_F and Fe_E-Fe_E pairs but also all possible permutations of O, OH, and H_2O pairs, as shown in Figure 4 of Michel et al. (2010). The lack of chemical selectivity of PDF is a major hindrance to determining unambiguously the polyhedral connectivity of ferrihydrite, and multi-elemental defective minerals in general (Fernandez-Martinez et al. 2010).

A coordination shell made of CN identical atoms at slightly different distances from the photoabsorber, that cannot be resolved into different subshells (e.g., CN1 at distance $R1$ and CN2 at distance $R2$, with CN1 + CN2 = CN), broadens the distribution of the absorber–neighbor distances. For small static disorder ($|R1 - R2| << R1,R2$), the multiple shell is equivalent to a single shell with coordination CN and mean distance $<R>$ = (CN1$R1$ + CN2$R2$)/CN, provided one introduces in the Debye-Waller factor the additional variance σ^2 = CN1CN2$|R1 - R2|^2$/CN^2 (Teo 1986; Manceau and Drits 1993). This analysis is applied first to the EXAFS spectrum of feroxyhite (δ-FeOOH), because each Fe octahedron shares a face like in hematite (Patrat et al. 1983; Drits et al. 1993b) and this polyhedral association can be resolved by EXAFS. Two spectra from six-line ferrihydrites, one recorded at room temperature (6Fh from Manceau 2009) and another at 30 K (6-Fh 30K from Manceau et al. 1993), are analyzed next to see if EXAFS can detect octahedra that share a common face in this mineral.

EXAFS analysis of feroxyhite

In the initial attempt, the feroxyhite spectrum was fit by fixing $CN_{O1} = CN_{O2}$ and $\sigma_{Fe1} = \sigma_{Fe2}$ and optimizing all other structural EXAFS parameters (Figs. 4a–5a). The hypothesis of $CN_{O1} = CN_{O2}$ is justified by the separation of the Fe-O and Fe-OH bond distances in α- and δ-FeOOH (Figs. 3a–3b). This fitting approach provided a reasonably good visual description of the data, except at 11.5 Å^{-1}. In addition, the Debye-Waller factor of the Fe shells was too high (σ_{Fe} = 0.125 Å) to capture all the distribution of absorber–neighbor distances in these shells. In the harmonic (i.e., Gaussian) approximation of the static disorder, the distribution of interatomic distances becomes questionable when σ is higher

◀**Figure 3.** Population histograms of the Fe-O/Fe-OH (first coordination shell only) and Fe-Fe distances up to 3.7 Å in ferric (oxyhydr)oxides and the fhyd6 and ferrifh models. The number of atomic pairs are for the asymmetric units of goethite, lepidocrocite, hematite (one Fe position or formula unit), and akaganeite (two Fe positions or formula units), and for half the unit cell of ferrifh and fhyd6 (5 Fe positions). Because the structure of feroxyhite is defective, the number of E (edge) and DC (double-corner) Fe-Fe pairs is not known precisely and was assumed to be the same as in hematite. Interatomic distances are counted in intervals of 0.05 Å. For ferrifh, being a mixture of 2Fh/6Fh, hematite, and maghemite, there is not enough information in the PDF data alone to result in a unique structural attribution in the 2.9–3.4 Å interval. The Fe-Fe correlation at 2.91 Å in fhyd6 is likely from shared faces. Crystallographic data from Blake et al. (1966), Hazemann et al. (1991), Drits et al. (1993b), Zhukhlistov (2001), Michel et al. (2007, 2010), and Takagi et al. (2010).

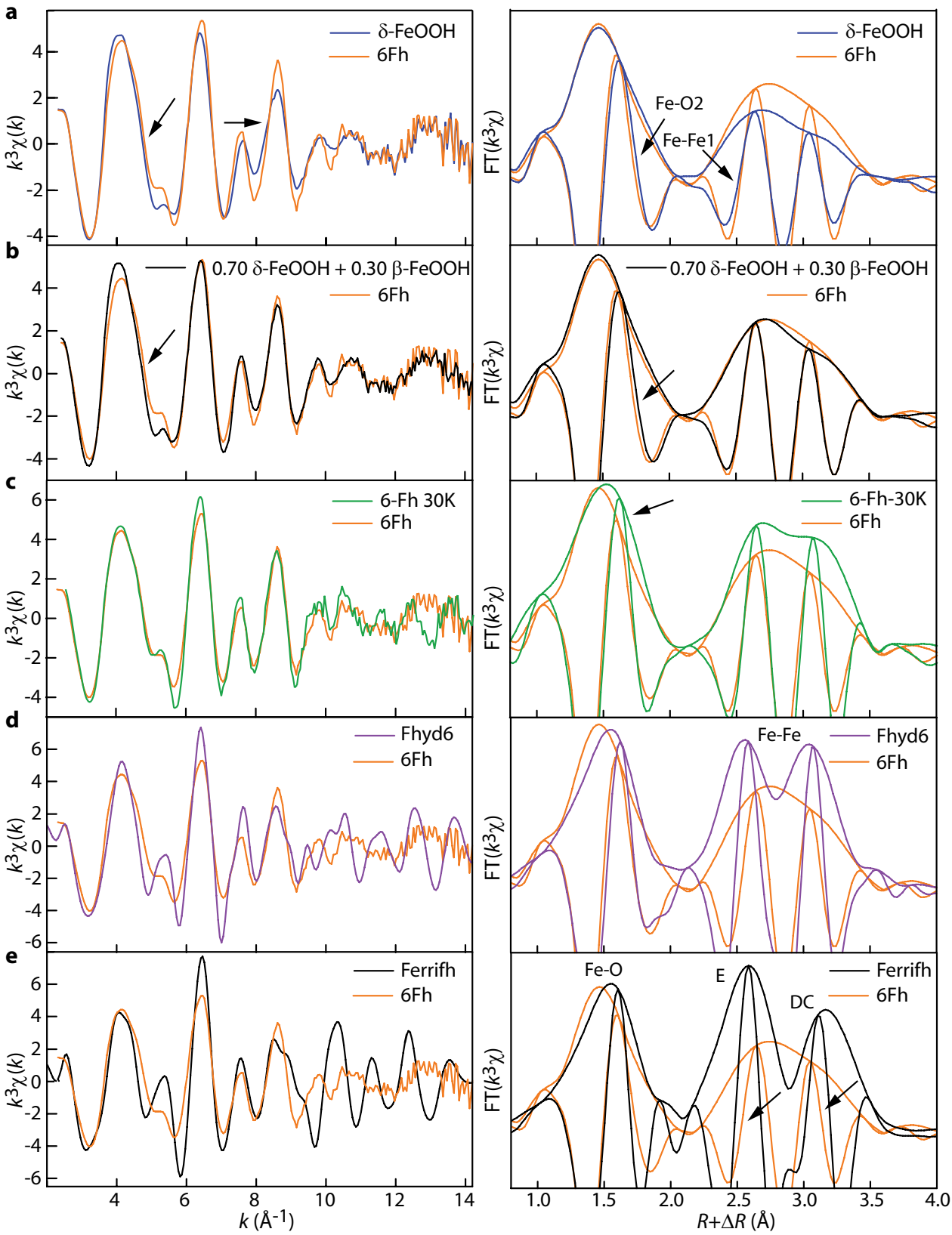

FIGURE 4. EXAFS spectra (**left**) and Fourier transforms (**right**) of feroxyhite (synthetic δ-FeOOH, experimental), six-line ferrihydrite (6Fh, experimental), a linear combination of 70% feroxyhite (containing some nanohematite) + 30% akaganeite (β-FeOOH), 6-Fh 30K (from Manceau and Drits 1993), and fhyd6 and ferrifh (calculated). The fhyd6 and ferrifh spectra were calculated ab initio using crystallographic data of Michel et al. (2007, 2010) and the method described by Manceau (2009). The HEXS fhyd6 and ferrifh models do not describe EXAFS data.

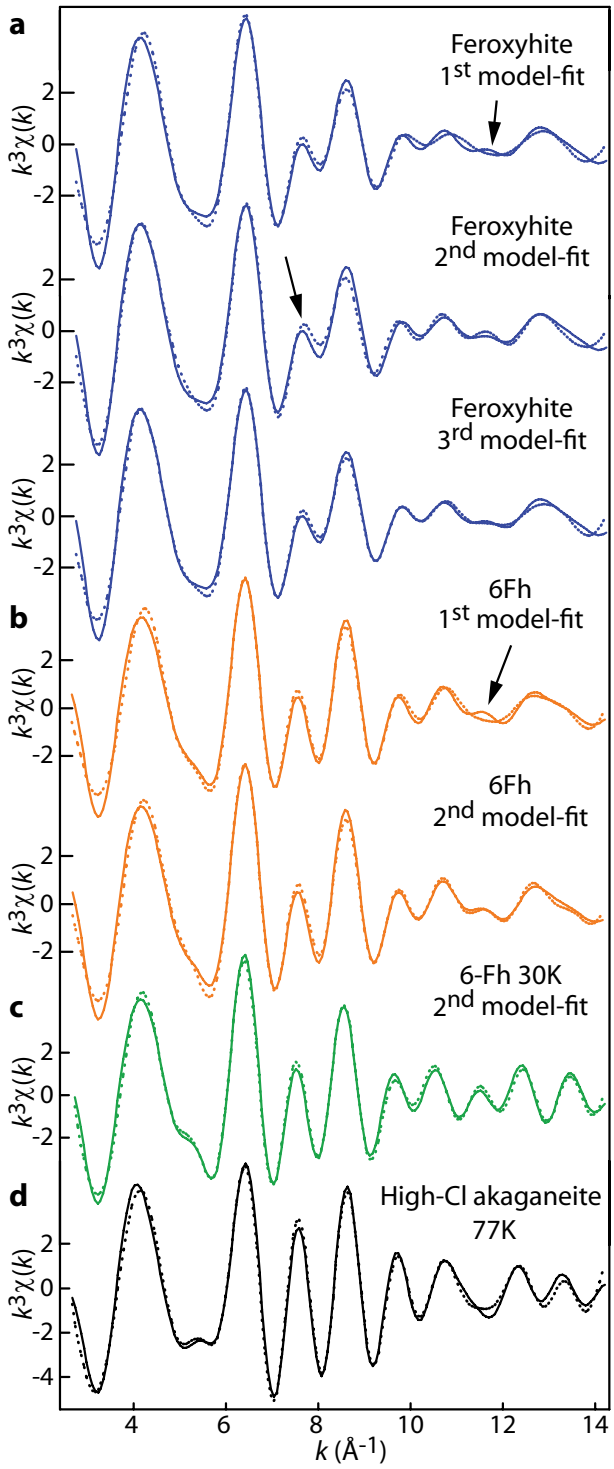

FIGURE 5. Multi-shell fit (dots) to Fourier-filtered Fe-O and Fe-Fe EXAFS data (lines) for feroxyhite, 6Fh, 6-Fh 30K, and high-Cl akaganeite. The fit parameters are listed in Tables 1 and the Supplementary materials[1]. For analytical details, see the Supplement.

than ~0.1 Å (Teo 1986; Crozier 1997). The beat feature at 11.5 Å^{-1} could be reproduced only when σ_{Fe1} and σ_{Fe2} were included as fitting parameters. However, the fit failed to converge: σ_{Fe1} = 0.196 Å and CN_{Fe1} = 20.9. Also, the fit did not reproduce the spectral signature at 7.60 Å^{-1}; this resonance occurs at 7.55 Å^{-1} in the model. Convergence was achieved by splitting the Fe1 into two subshells at 2.89 and 3.03 Å, in agreement with XRD. This produced an excellent description of the data over the entire k range with all fit parameters being physically and structurally meaningful (Tables 1 and Supplementary materials[1]).

The EXAFS pair distribution function calculated from the optimized R_j and σ_j values matches, within precision (Supplementary Table 1[1]), the histograms of the Fe_F-Fe_F and Fe_E-Fe_E pairs in the structure, but not R_{O2} nor CN_{FeDC} (Fig. 6a). At long distance there is an apparent loss of coordination (CN_{Fe2} = 1.4 instead of approximately 3) typical of broad, generally asymmetric, distributions in disordered systems (Marcus et al. 1986). The R_{O2} value of the XRD model is clearly too high.

EXAFS analysis of six-line ferrihydrite

Two fitting methods were tried to extract the most structural information from the 6Fh spectrum (Figs. 4b–5b). The first method was adapted from the analysis of two- and six-line ferrihydrite (samples 2L FH and 6L FH) by Toner et al. (2009). In this study, the two oxygen subshells were assumed to contain the same number of atoms ($CN_{O1} = CN_{O2}$), and R_j and σ_j were adjusted. The optimal σ values were almost the same for the two Fe shells of 6L FH (0.089–0.095 Å, Table 1). Therefore, 6Fh was fit initially with the following constraints: $CN_{O1} = CN_{O2}$ and $\sigma_{Fe1} = \sigma_{Fe2}$. The Debye-Waller factor converged to σ_{Fe} = 0.098 Å and the model-fit reproduced the data to k_{max} = 14.2 Å^{-1}, except for the beat node pattern at 11.5 Å^{-1} (Fig. 5b). When the two σ parameters were not constrained during minimization, σ_{Fe1} converged to 0.109 Å, σ_{Fe2} to 0.081 Å, and the beat node pattern was reproduced. Toner et al. (2009) obtained the same type of fit for 2L FH (their Fig. 9b), with σ values close to those calculated here: σ_{Fe1} = 0.114 Å and σ_{Fe2} = 0.077 Å (Table 1). This second fit method is clearly better because it is the only one (others were tested unsuccessfully) that reproduced data up to 14.2 Å^{-1}. The optimal EXAFS values for 6Fh are CN_{Fe1} = 3.4 ± 1.3, R_{Fe1} = 3.02 ± 0.02 Å, σ_{Fe1} = 0.11 ± 0.07 Å, and CN_{Fe2} = 1.8 ± 1.1, R_{Fe2} = 3.42 ± 0.01 Å, σ_{Fe2} = 0.08 ± 0.05 Å (Table 1, Supplementary materials[1]). How these values relate to the polyhedral structure of Fh is examined next.

A CN_{Fe1}/CN_{Fe2} ratio of 3.4/1.8 = 1.9 is incompatible with the framework structure of Fe (oxyhydr)oxides (Manceau and Combes 1988). For example, goethite and akaganeite have CN_{Fe1}/CN_{Fe2} = 2/(2+4) = 0.3 (Figs. 3b–3c). Only lepidocrocite has CN_{Fe1}/CN_{Fe2} > 1, but its bonding environments cannot be dominant in Fh because lepidocrocite has no Fe-Fe pairs at ~3.4 Å from the sharing of DC and has long-distance corner-sharing (C) pairs at ~3.9 Å not observed on the PDF, as stated previously. The limits on polyhedral coordination emplaced by crystal-chemical rules show that CN_{Fe2} is underestimated, as seen previously in the EXAFS analysis of feroxyhite. By analogy to feroxyhite, as many as ~50% of the Fe atoms in the DC shell may be "lost." Thus, the Fe2 shell may contain on average from 3 to 4 Fe neighbors, instead of 1.8 detected by EXAFS.

In contrast, the relatively high number of Fe1 neighbors (CN_{Fe1} = 3.4 ± 1.3; σ = 0.11 Å) from the second model-fit of 6Fh suggest that EXAFS captures most of the distribution of interatomic distances in this shell. Therefore, the number of missing Fe1 atoms probably does not exceed the precision

TABLE 1. EXAFS parameters from the multi-shell fits of ferrihydrite

	Fe-O1			Fe-O2			Fe-Fe1			Fe-Fe2/Fe3				
	CN	*R* (Å)	σ (Å)	CN	*R* (Å)	σ (Å)	CN	*R* (Å)	σ (Å)	CN	*R* (Å)	σ (Å)	Δ*E*	*Res*
Feroxyhite, 1st model-fit	2.8*	1.93	0.064	2.8*	2.07	0.066	3.7	3.02	**0.125***	3.0	3.40	**0.125***	−0.7	17
2nd model-fit	2.8*	1.93	0.064*	2.8*	2.07	0.064*	**20.9**	3.06	**0.196**	3.6	3.40	0.110	0.3	15.0
3rd model-fit	2.8*	1.93	0.064*	2.8*	2.07	0.064*	1.0‡	2.89	0.093*					
							1.9	3.03	0.093*	1.4	3.42	0.093*	−0.5	12.6
6Fh, 1st model-fit	2.6*	1.92	0.055	2.6*	2.05	0.063	2.4	3.02	0.098*	2.6	3.42	0.098*	−0.3	13.9
2nd model-fit	2.6*	1.92	0.055	2.6*	2.05	0.063	3.4	3.02	**0.109**	1.8	3.42	0.081	−0.5	12.1
6L FH†	3.3*	1.93	0.055	3.3*	2.07	0.077	3.0	3.03	**0.095**	2.4	3.43	0.089	–	–
2L FH†	2.7*	1.92	0.055	2.7*	2.04	0.071	3.5	3.05	**0.114**	1.4	3.45	0.077	–	–
6-Fh 30K, 1st model-fit	**5.1***	1.99	0.10	**5.1***	2.19	**0.18**	4.0	3.02	**0.114**	1.4	3.45	0.056	3.1	10.3
2nd model-fit	5.1	1.98	0.09*	0.9	2.15	0.09*	3.8	3.02	**0.109**	1.6	3.44	0.063	0.9	11.3
High-Cl akaganeite 77K	3.3*	1.95	0.079	3.3*	2.12	0.091	2.0	3.03	0.077*	0.9	3.34	0.077*	0.8	13.1
										2.2	3.47	0.077*		

Notes: CN is the effective number of atomic pairs seen by EXAFS, *R* is the interatomic distance, σ is the standard deviation of the distance distribution, Δ*E* is the threshold energy correction in eV, and *Res* is the fit residual defined as $[\Sigma\{|\chi_{exp} - \chi_{fit}|\}/\Sigma\{|\chi_{exp}|\}] \times 100$. The many body amplitude-reduction factor S_0^2 was fixed to 0.8.
* Constrained to the same value for the two shells.
† Results from Toner et al. (2009).
‡ Fixed to the crystallographic value of a defect-free feroxyhite.

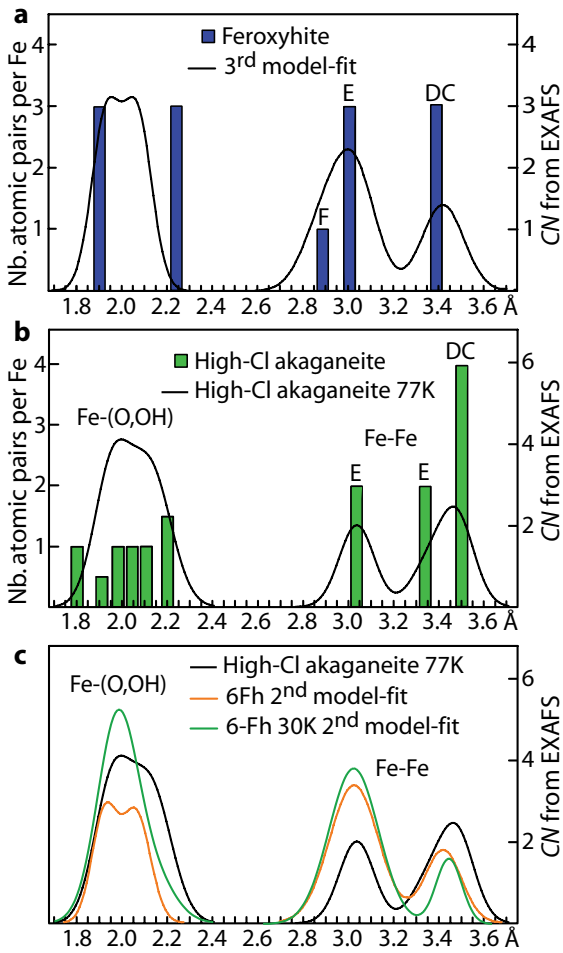

FIGURE 6. Radial distributions of the Fe-O and Fe-Fe distances for feroxyhite, high-Cl akaganeite at 77 K, and six-line ferrihydrite derived from EXAFS (solid lines) and from diffraction for feroxyhite and high-Cl akaganeite (histogram). To facilitate the comparison of EXAFS and diffraction results, the diffraction distances in plots **a** and **b** were not rounded to 0.05 Å, in contrast to Figure 3.

on CN_{Fe1} (1.3) (i.e., 3.4 + 1.3 = 4.7). This maximum is more likely 4, as in goethite/akaganeite and hematite. The Fe1 shell in γ-FeOOH has CN = 6, but this high number is balanced for steric reasons by a small number of Fe2 atoms (2) at a longer distance of ~3.9 Å.

The best-fit Gaussian model of the Fe1 shell is centered at R_{Fe1} = 3.02 Å with a width of σ_{Fe1} = 0.11 Å. Approximately 15% [(1 − σ)/2] of the Fe1 atoms are at least at 0.11 Å from the geometric mean, i.e., at *R* < 2.91 Å from another Fe1. This distance range is typical of a shared face. The 6Fh sample has a wider pair distribution function than high-Cl akaganeite in this *R* region (σ_{Fe1} = 0.077 Å, Table 1, Figs. 5d and 6b), confirming the sensitivity of EXAFS to face-sharing octahedra in Fh. The number of F linkages per Fe is estimated as approximately 0.15 × 3.4 = 0.5 (15% probability × CN_{Fe1}). Although face-sharing octahedra in Fh were documented previously using EXAFS (Combes et al. 1990; Fig. 4 in Manceau and Drits 1993), the analysis presented here is new and serves as a good demonstration of how σ can be used to extract meaningful structural information in a well-conditioned and constrained system.

Evidence for mixed akaganeite/feroxyhite-types of polyhedral linkages in ferrihydrite

In the three-phase model of Drits et al. (1993a), shared faces exist in the d-phase and hematite, but not in the f-phase (Fig. 1). Because the d-phase is more abundant than hematite and is structurally close to δ-FeOOH, the EXAFS spectrum of 6Fh should have similarities to that of feroxyhite. The two spectra and Fourier transforms are shown in Figure 4a. EXAFS reveals no fundamental local structural differences between the two phases. The first oscillation of 6Fh is broadened on its right tail, thus shifting the maximum of the 5.35 $Å^{-1}$ hump for feroxyhite to the apparent value of 5.30 $Å^{-1}$. On the Fourier transform (Fig. 4a, right), the lower frequency of the first oscillation of 6Fh manifests itself as a shortening of the Fe-O2 pair.

The second noticeable difference between the 6Fh and feroxyhite spectra is a downshift of the resonance at 7.60 $Å^{-1}$ for feroxyhite to 7.55 $Å^{-1}$ for 6Fh. In *R* space, this difference is seen as a shortening of the Fe-Fe1 pair in feroxyhite. This reduction in distance can be explained as follows: Each Fe octahedron shares one face (assuming no defect) with another octahedron along the direction of the -◊-◊-Fe-Fe-◊-◊-Fe-Fe chains in feroxyhite (Fig. 1), and this number is approximately 0.5 on average in 6Fh.

These observations and general considerations on the poly-

hedral structure of the f-phase (Fig. 1) suggest that the short-range radial distribution of the Fe-O and Fe-Fe distances in ferrihydrite may be approximated by a mixture of feroxyhite/hematite (~d-phase) and goethite/akaganeite (~f-phase). Linear least-squares combination fitting of the experimental EXAFS spectra for these references to the 6Fh spectrum was conducted to further explore this possibility. This analysis revealed that the Fe-Fe correlations could be approximated astonishingly well with a simple combination of 70 ± 10% feroxyhite containing some nanohematite and 30 ± 10% akaganeite (Figs. 4b and 7). Adding a third component marginally improved the fit. Linear combinations with either well-crystallized hematite or goethite in a two-component fit were not successful, but provided additional information on the structural meaning of the shift of the resonance at k ~ 7.6 Å^{-1} in feroxyhite relative to 6Fh (Fig. 4a). This feature is at 7.65 ± 0.01 Å^{-1} in hematite, thus shifted even more to the right than in feroxyhite. Formally, both feroxyhite and hematite have one F linkage per Fe octahedron, therefore the resonances of the F linkage are expected to be at the same position. The defective nature of the feroxyhite structure may explain the observed difference.

The proportions of the feroxyhite-type (~70%) and akaganeite-type (~30%) of octahedral linkages have no reason to be the same among the varieties of ferrihydrites, and should vary in particular with crystallinity (e.g., 6Fh vs. 2Fh), thus sample preparation including the temperature of synthesis and the aging time in solution. Generally, 6Fh has more shared faces, hence feroxyhite-type fragments, than 2Fh (Combes et al. 1990; Manceau and Drits 1993), because it is synthesized usually between 75 and 90 °C and is a precursor to the solid-state formation of hematite (Schwertmann and Cornell 1991; Cornell and Schwertmann 2003). As shown in Figure 7, the proportion of feroxyhite-type local coordination can be estimated also from the shape of the main diffraction peak of 6Fh at 2.50–2.55 Å.

The akaganeite-type of local structure identified here by EXAFS actually occurs in the f-phase (Fig. 1). In this phase, octahedra are linked together in short single and double chains, which are cross-linked irregularly to form akaganeite-like and goethite-like nano-domains. The Fe atoms across the A anionic planes are separated by about 3.30 Å, like those across the OH_{sh}-OH_{sh} edges in α/β-FeOOH (~3.30–3.35 Å). By analogy to the bonding environment of Fe in α/β-FeOOH, the A planes were assumed to contain predominantly hydroxyls, and the B and C planes mainly O atoms (Drits et al. 1993a). This assumption is also structurally consistent with the Fe_E-$Fe1_E$ separation of 2.96 Å in the Drits model, because the shared edges are with one OH_{sh} from an A plane and an O_{sh} from a B or C plane, not with two OH_{sh}. Like for edges, electrostatics dictate that the Fe_{DC}-$Fe2_{DC}$ separation is longer when the apices are hydroxyls (~4.4 Å) rather than O atoms (~3.50 Å). In α/β-FeOOH, octahedral chains are cross-linked through O atoms only, and the Fe_{DC}-$Fe2_{DC}$ separation is 3.45–3.52 Å. These crystal-chemical considerations show that the f-phase model is structurally sound, despite the high degree of uncertainty in the details of its crystallographic structure due to the relatively poor crystallinity (i.e., high defect density) of ferrihydrite. In this case Pauling's distortion rule is not violated, in contrast to the ferrifh model (Michel et al. 2010).

Evidence for long-distance Fe-O pairs in ferrihydrite

The akaganeite + feroxyhite (with minor nanohematite) model fails, however, to reproduce the Fe-O correlations of the EXAFS spectrum for 6Fh seen at k ~5 Å^{-1} (k space) and on the imaginary part at $R + \Delta R$ ~ 1.7–1.8 Å of the Fourier transform (R space; Fig. 4b). The Fe coordination is usually described with one or two oxygen sub-shells and an average bond length of R = 1.96–1.99 Å (one shell) to 1.98–2.02 Å (two shells) (Combes et al. 1989, 1990; Waychunas et al. 1993; Rose et al. 1997; O'Day et al. 2004; Ulrich et al. 2006; Majzlan et al. 2007; Mikutta et al. 2008, 2010; Toner et al. 2009; Carta et al. 2009; Voegelin et al. 2010). The lower EXAFS distances, which approach the shortest Fe-O distance in hematite (1.95 Å), are associated generally with a loss of oxygen neighbors (CN_O < 6) and high σ values without a noticeable trend between R and CN. Disorder, as discussed previously for the Fe-Fe pairs, is the most likely reason to the loss of O atoms based on the well-known sensitivity of EXAFS to structural disorder (Teo 1986). Some of the "lost" atoms may be recovered by decreasing the atomic motion at low temperature, especially when the distribution of distances is anharmonic, which seems to be the case from the histogram of the Fe-O distances in fhyd6 that is from pure ferrihydrite (Fig. 3d). Therefore, the low-temperature (30 K) spectrum of the 6-Fh 30K sample studied by Manceau and Drits (1993) was re-analyzed for both the Fe-O and Fe-Fe pairs. Only the Fe-Fe pairs had been analyzed previously.

The ferrihydrite spectrum is more resolved at high k and has a higher amplitude at cryogenic than at room temperature, as expected when the thermal motion of atoms is diminished (Fig.

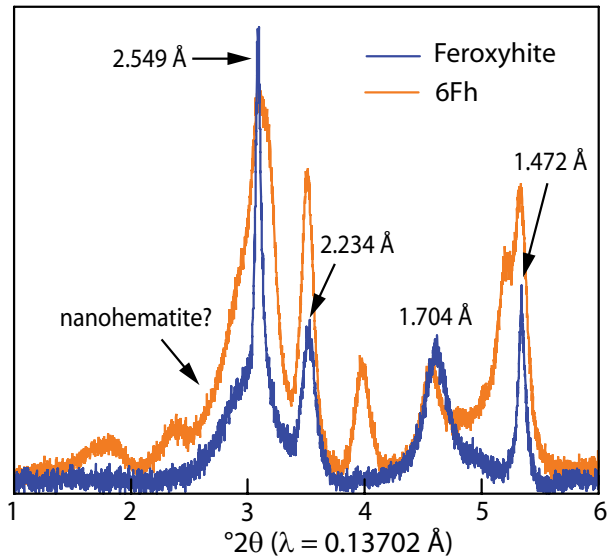

FIGURE 7. Experimental X-ray diffraction patterns for six-line ferrihydrite (6Fh from Manceau 2009) and feroxyhite (Ferox from Drits et al. 1993b). The feroxyhite-like structure of the d-phase is responsible for the asymmetry of the peak maximum for 6Fh. The shape of this peak depends on the relative proportions of the f- and d-phases. The composite nature of this peak is strong evidence that six-line ferrihydrite cannot be described fully with one periodic structural model, and predicts that well-crystallized ferrihydrite contains seven lines. The broad hump at 2.8–3.0 °2θ (~2.70 Å) in both 6Fh and feroxyhite may represent nanohematite (Fig. 7 in Drits et al. 1993b).

4c). In real space, there is a shift of the maximum and modification of the shape of the Fe-O peak. The newly detected Fe-O long bond is unmistakable when CN_{O1} and CN_{O1} are constrained to be identical during the fit, as for the room-temperature data: the regression yields unrealistic values of $CN_{O1} = CN_{O2} = 5.1$ and $\sigma_{O2} = 0.18$ Å (Table 1). Meaningful values consistent with room-temperature results were obtained by optimizing the two CN_O parameters, and fixing $\sigma_{O1} = \sigma_{O2}$ to minimize correlations. The total pair distribution function of the Fe-O pairs is now asymmetrical on its right tail with 5.1 O1 at 1.98 Å and 0.9 O2 at 2.15 Å (Fig. 6c). The weighted bond length (2.00 Å) is nearly the same as the average $^{VI}Fe^{3+}$-O distance in crystal structures (2.015 Å; Brown and Altermatt 1985; Manceau 2010). The dominant Fe-O correlation is at 1.98 Å like in schwertmannite (Fernandez-Martinez et al. 2010). The number of Fe2 atoms is still too low (1.6), partly because of the small particle size, extensive disorder, and large range of Fe-Fe2 distances. Some may be recovered by splitting the Fe2 shell, but with the risk of overfitting the data and introducing strong correlations between parameters.

The higher sensitivity of EXAFS to longer Fe-O bonds at cryogenic temperature is also clearly seen on the Fourier transforms of high-Cl akaganeite obtained at room and liquid nitrogen temperatures (Supplementary Fig. 2a[1]). The 77 K spectrum has a distinctive shoulder at $R + \Delta R = 1.8$–1.9 Å from distant O atoms. The histogram of the Fe-O distances derived from XRD shows a wide range of distances from 1.80 Å to 2.20 Å (Fig. 6b). This metrical spread can be represented by two Gaussians centered at 1.95 Å ($\sigma = 0.079$ Å) and 2.12 Å ($\sigma = 0.091$ Å, Table 1). The difference of $<d(\text{Fe-O1})> = 1.98 - 1.95 = 0.03$ Å between 30 K ferrihydrite and 77 K akaganeite is reflected phenomenologically in the shift of the Fe-O maxima of their Fourier transforms (Supplementary Fig. 2b[1]).

Concluding remarks

The anion packing of akdalaite is ABAC like the f-phase of the Drits model. A main difference between the two models, however, is the site occupancy of Fe, which is 20% tetrahedral in akdalaite and 100% octahedral in the other f-phase (Supplementary materials[1]). The coexistence of two coordinations is a source of complication in refining PDF data (Farrow et al. 2007; Manceau 2010). The asymmetric unit of the akdalaite model has three Fe and four O atoms for a total of 10 independent crystallographic positions refined in the PDF analysis. Atomic motions and instrumental parameters must also be adjusted. In contrast with the akdalaite model, the f-phase was refined with only one crystallographic parameter, the *z* position of Fe. Its asymmetric unit contains one Fe in the 4f position (1/3, 2/3, z) and two O atoms at the special positions of undeformed ABAC close packing. Although different *z* values were obtained with X-rays (0.15; Drits et al. 1993a), neutrons (0.136; Jansen et al. 2002), and electrons (0.13; Cowley et al. 2000), the f-phase gave the best match between experiment and model for all three techniques. The XRD pattern calculated with this simple model with a low degree of freedom is extremely close to the data (Fig. 2). The main difference is the maximum of the most intense reflection, which is at ~2.48 Å in the model and ~2.54–2.55 Å in data. A small shift of one or a set of reflections is typical of scattering effects from stacking faults, as commonly observed in defective layer compounds (Drits and Tchoubar 1990; Lanson et al. 2002). The shift issue was solved by adding random sequences of enantiomorphous ABA and ACA layers, the so-called d-phase (Fig. 7). The second difference was the strong asymmetry at low *Q* of the ~2.50–2.55 Å peak. Because hematite has its strongest reflection at 2.70 Å and is a common mineral frequently present as impurities in natural Fe oxyhydroxides, its occurrence was suggested. The diffuse scattering intensity in this *Q* region could be reproduced by assuming nanohematite crystallites with an average domain size of 10 Å in diameter and 14 Å in thickness. Nanohematite also is detected on the XRD pattern of feroxyhite (Fig. 7) used as reference with akaganeite to reconstruct the EXAFS spectrum of 6Fh (Fig. 4b).

The d-phase, which was introduced in the Drits model to match the position of the most intense diffraction peak, is not really a separate phase because the ABA and ACA fragments have a clear genetic relationship with the ABAC periodic stack of the f-phase. Because the ABA and ACA fragments are enantiomorphous, adding this component introduced only one new crystallographic parameter, the *z* position of the Fe atoms, that is different from that in the f-phase. In summary, the Drits Fh model is in essence "single-phase," with varying degrees of well-defined disorder represented by variable proportions of the d-phase. In some samples, the d-phase may dominate, as suggested by EXAFS spectroscopy for 6Fh and in the Fe domains of iron-rich natural vernadite (called "Fe-vernadite;" Manceau and Combes 1988; Manceau et al. 1992). In this case, the main diffraction maximum at 2.50–2.55 Å should be asymmetric and peak at ~2.55 Å (Fig. 7). It is possible, however, that the d- and f-phases coexist and are well crystallized, in which case this compound would exhibit seven diffraction lines.

A model is considered good if it accurately describes a large group of observations using only a few arbitrary elements. Applied to data simulations, this paradigm shows that the Drits model is a good model for the following reasons. (1) It has the flexibility to describe the known occurrences of ferrihydrite, whether geological, biogenic (ferritin), or synthetic. (2) It is consistent with diffraction and spectroscopy results (Combes et al. 1989, 1990; Manceau et al. 1990; Pankhurst and Pollard 1992; Manceau and Drits 1993; Shinoda et al. 1994; Waychunas et al. 1993, 1996; Manceau and Gates 1997; Janney et al. 2000, 2001; Cowley et al. 2000; Jansen et al. 2002; De Grave et al. 2005; Pan et al. 2006, 2009, 2010). And (3) it contains a limited number of parameters. When one has the choice between two models to explain a set of observations, the law of parsimony recommends choosing the one that introduces the fewest assumptions.

Nevertheless, the Drits model still needs refinement. For example, the atomic positions of Fe and O atoms, and the ordering of O and OH within and among the anionic planes are not well understood. The Fe-O1 and Fe-O2 distances in the f-phase deduced from XRD, neutron and electron diffraction are 1.95 and 2.216 Å, 2.01 and 2.13 Å, and 2.07 and 2.12 Å, respectively. Their mean values are too high for a $^{VI}Fe^{3+}$-(O,OH) coordination, and the diffraction bond lengths do not coincide well with the EXAFS distances. For comparison, the akaganeite structure of MacKay (1962) has one Fe position, two O positions, and $<d(\text{Fe-O})> = 2.08$ Å. This structure was refined by Post et al. (2003) and Tagaki et al. (2010) in a lower symmetry space group with two

Fe and four O positions. The mean bond length is 2.03–2.04 Å, which is more realistic. Similar to akaganeite, the atomic sites of the f-phase could be split into nonequivalent positions by choosing a space group with a lower symmetry than $P\bar{3}1c$. However, this refined model may not be more precise, because increasing the number of degrees of freedom in the refinement may introduce correlations between adjustable parameters and consequent overfitting of data.

The displacement of Fe cations away from the A planes suggests that these planes contain predominantly OH groups, because the reduced effective charge for oxygen in OH^- gives rise to longer bond lengths. Reciprocally, the B and C planes are assumed to hold most of the O^{2-}. Similar displacements are observed in the other oxyhydroxides (Fig. 1), with the important difference that the O and OH are ordered *within* the anionic planes (Fig. 2 in Manceau et al. 2000), not from one plane to another as suggested in the Drits model. This question could be addressed in more detail using neutron diffraction on deuterated ferrihydrite. Neutron diffraction will also be more sensitive to the ratio of O to OH in the structure than XRD.

With the caveat of the poor sensitivity of XRD to the positions of O and OH in the structure, some general observations about the O/OH ratio are appropriate. In the Drits model, the occupancy of the anion sites is 1.0 for the A planes that contain predominantly OH, and 0.85 for the B and C planes that contain predominantly O atoms. If each plane contained only OH or O, the total weight loss from dehydroxylation should be 10.4%. This value is consistent with the weight losses of 10.5% and 15% measured for 6Fh between 100–120 °C and 800–1000 °C by thermogravimetric analysis (Saleh and Jones 1984; Eggleton and Fitzpatrick 1988). The akdalaite-like model $[Fe_{10}O_{14}(OH)_2]$ has 2.2 wt% H_2O-equivalent structural OH, much less than experimental values, even after correction of particle size effects (Hiemstra and van Riemsdijk 2009). The anomalously H-poor content of the akdalaite-like model also was pointed out by Rancourt and Meunier (2008).

Acknowledgments

Dogan Paktunc, John Parise, and one anonymous reviewer offered helpful comments on the manuscript. EXAFS measurements at room temperature were performed on beamline 10.3.2 at the Advanced Light Source (ALS, Berkeley). The ALS is supported by the Director, Office of Energy Research, Office of Basic Energy Sciences, Materials Sciences Division of the U.S. Department of Energy, under contract no. DE-AC02-05CH11231.

References cited

Barron, V., Torrent, J., and De Grave, E. (2003) Hydromaghemite, an intermediate in the hydrothermal transformation of 2-line ferrihydrite into hematite. American Mineralogist, 88, 1679–1688.

Bino, A., Ardon, M., Lee, D., Spingler, B., and Lippard, S.J. (2002) Synthesis and structure of $[Fe_{13}O_4F_{24}(OMe)_{12}]^{5-}$: The first open-shell Keggin ion. Journal of the American Chemical Society, 124, 4578–4579.

Blake, R.L., Hessevick, R.E., Zoltai, T., and Finger, L.W. (1966) Refinement of the hematite structure. American Mineralogist, 51, 123–129.

Brown, I.D., and Altermatt, D. (1985) Bond-valence parameters obtained from a systematic analysis of the Inorganic Crystal Structure Database. Acta Crystallographica, B, 41, 244–247.

Campbell, A.S., Schwertmann, U., and Campbel, P.A. (1997) Formation of cubic phases on heating ferrihydrite. Clay Minerals, 32, 615–622.

Carta, D., Casula, M.F., Corrias, A., Falqui, A., Navarra, G., and Pinna, G. (2009) Structural and magnetic characterization of synthetic ferrihydrite nanoparticles. Materials Chemistry and Physics, 113, 349–355.

Combes, J.M., Manceau, A., Calas, G., and Bottero, J.Y. (1989) Formation of ferric oxides from aqueous solutions: a polyhedral approach by X-ray absorption spectroscopy. I. Hydrolysis and formation of ferric gels. Geochimica et Cosmochimica Acta, 53, 583–594.

Combes, J.M., Manceau, A., and Calas, G. (1990) Formation of ferric oxides from aqueous solutions: a polyhedral approach by X-ray absorption spectroscopy. II. Hematite formation from ferric gels. Geochimica et Cosmochimica Acta, 54, 1083–1091.

Cornell, R.M. and Schwertmann, U. (2003) The Iron Oxides: Structure, Properties, Reactions, Occurrence and Uses, VCH, New York.

Corrias, A., Ennas, G. Mountjoy, G., and Paschina, G. (2000) An X-ray absorption spectroscopy study of the Fe K edge in nanosized maghemite and in Fe_2O_3-SiO_2 nanocomposites. Physical Chemistry Chemical Physics, 2, 1045–1050.

Cowley, J.M., Janney, D.E., Gerkin, R.C., and Buseck, P.R. (2000) The structure of ferritin cores determined by electron nanodiffraction. Journal of Structural Biology, 131, 210–216.

Crozier, E.D. (1997) A review of the current status of XAFS spectroscopy. Nuclear Instruments and Methods in Physics Research Section B Beam Interactions with Materials and Atoms, 133, 134–144.

de Boer, C.B. and Dekkers, M.J. (2001) Unusual thermomagnetic behaviour of haematites: neoformation of a highly magnetic spinel phase on heating in air. Geophysical Journal International, 144, 481–494.

De Grave, E., Vandenberghe, R.E., and Dauwe, C. (2005) ILEEMS: Methodology and applications to iron oxides. Hyperfine Interactions, 161, 147–160.

de Juan, A. and Tauler, R. (2003) Chemometrics applied to unravel multicomponent processes and mixtures. Revisiting latest trends in multivariate resolution. Analytica Chimica Acta, 500, 195–210.

Drits, V.A. and Tchoubar, C. (1990) X-ray Diffraction by Disordered Lamellar Structures: Theory and applications to microdivided silicates and carbons. Springer-Verlag, Berlin.

Drits, V.A., Sakharov, B.A., Salyn, A.L., and Manceau, A. (1993a) Structural model for ferrihydrite. Clay Minerals, 28, 185–208.

Drits, V.A., Sakharov, B.A., and Manceau, A. (1993b) Structure of feroxyhite as determined by simulation of X-ray diffraction curves. Clay Minerals, 28, 209–222.

Drits, V.A., Gorshkov, A.I., Sakharov, B.A., Salyn, A.L., and Manceau, A. (1995) Ferrihydrite and its phase transitions during heating in the oxidizing and reducing environments. Lithology and Mineral Resources, 1, 68–75 (translated from Litologiya, 1, 76–84, 1995).

Eggleton, R.A. and Fitzpatrick, R.W. (1988) New data and a revised structural model for ferrihydrite. Clays and Clay Minerals, 36, 111–124.

Farrand, W.H., Glotch, T.D., Rice, J.W., Hurowitz, J.A., and Swayze, G.A. (2009) Discovery of jarosite within the Mawrth Vallis region of Mars: Implications for the geologic history of the region. ICARUS, 204, 478–488.

Farrow, C.L., Juhas, P., Liu, J.W., Bryndin, D., Bozin, E.S., Bloch, J., Proffen, T., and Billinge, S.J.L. (2007) PDFfit2 and PDFgui: computer programs for studying nanostructure in crystals. Journal of Physics: Condensed Matter, 19, 335219.

Fernandez-Martinez, A., Timon, V., Roman-Ross, G., Cuello, G.J., Daniels, J.E., and Ayora, C. (2010) The structure of schwertmannite, a nanocrystalline iron oxyhydroxysulfate. American Mineralogist, 95, 1312–1322.

Flynn, C.M. (1984) Hydrolysis of inorganic iron (III) salts. Chemical Reviews, 84, 31–41.

Fortin, D. and Langley, S. (2005) Formation and occurrence of biogenic iron-rich minerals. Earth-Science Reviews, 72, 1–19.

Greaves, C. (1983) A powder neutron diffraction investigation of vacancy ordering and covalence in γ-Fe_2O_3. Journal of Solid State Chemistry, 49, 325–333.

Guyodo, Y., Banerjee, S.K., Penn, R.L., Burleson, D., Berauo, T.S., Seda, T., and Solheid, P. (2006) Magnetic properties of synthetic six-line ferrihydrite nanoparticles. Physics of the Earth and Planetary Interiors, 154, 222–233.

Hazemann, J.L., Berar, J.F., and Manceau, A. (1991) Rietveld studies of the aluminium-iron substitution in synthetic goethite. Materials Sciences Forum, 79-82, 821–826.

Hiemstra, T. and van Riemsdijk, W.H. (2009) A surface structural model for ferrihydrite I: Sites related to primary charge, molar mass, and mass density. Geochimica et Cosmochimica Acta, 73, 4423–4436.

Hwang, S.L., Shen, P.Y., Chu, H.T., and Yui, T.F. (2006) A new occurrence and new data on akdalaite, a retrograde mineral from UHP Whiteschist, Kokchetav Massif, Northern Kazakhstan. International Geology Review, 48, 754–764.

Jambor, J.L. and Dutrizac, J.E. (1998) Occurrence and constitution of natural and synthetic ferrihydrite, a widespread iron oxyhydroxide. Chemical Reviews, 98, 2549–2586.

Janney, D.E., Cowley, J.M., and Buseck, P.R. (2000) Structure of synthetic 2-line ferrihydrite by electron nanodiffraction. American Mineralogist, 85, 1180–1187.

——— (2001) Structure of synthetic 6-line ferrihydrite by electron nanodiffraction. American Mineralogist, 86, 327–335.

Jansen, E., Kyek, A., Schafer, W., and Schwertmann, U. (2002) The structure of six-line ferrihydrite. Applied Physics A-Materials Science and Processing, 74, S1004–S1006.

Juhas, P., Cherba, D.M., Duxbury, P.M., Punch, W.F., Billinge, S.J.L. (2006) Ab

initio determination of solid-state nanostructure. Nature, 440, 655–658.
Lanson, B., Drits, V.A., Gaillot, A.C., Silvester, E.J., Plançon, A., and Manceau, A. (2002) Structure of heavy metal sorbed birnessite. 1. Results from X-ray diffraction. American Mineralogist, 87, 1631–1645.
Liu, Q., Barron, V., Torrent, J., Eeckhout, S.G., Deng, C. (2008) Magnetism of intermediate hydromaghemite in the transformation of 2-line ferrihydrite into hematite and its paleoenvironmental implications. Journal of Geophysical Research, 113, 1–12.
MacKay, A.L. (1962) β-ferric oxyhydroxide-akaganéite. Mineralogical Magazine, 33, 270–280.
Majzlan, J., Lalinska, B., Chovan, M., Jurkovic, L., and Milovska, S. (2007) The formation, structure, and ageing of As-rich hydrous ferric oxide at the abandoned Sb deposit Pezinok (Slovakia). Geochimica et Cosmochimica Acta, 71, 4206–4220.
Malinowski, E.R. (1991) Factor Analysis in Chemistry. Wiley, New York.
Manceau, A. (2009) Evaluation of the structural model for ferrihydrite derived from real-space modeling of high-energy X-ray diffraction data. Clay Minerals, 44, 19–34.
——— (2010) PDF analysis of ferrihydrite and the violation of Pauling's Principia. Clay Minerals, 45, 225–228.
Manceau, A. and Combes, J.M. (1988) Structure of Mn and Fe oxides and oxyhydroxides: a topological approach by EXAFS. Physics and Chemistry of Minerals, 15, 283–295.
Manceau, A. and Drits, V.A. (1993) Local structure of ferrihydrite and feroxyhite by EXAFS spectroscopy. Clay Minerals, 28, 165–184.
Manceau, A. and Gates, W. (1997) Surface structural model for ferrihydrite. Clays and Clay Minerals, 43, 448–460.
Manceau, A., Combes, J.M., Calas, G., Eggleton, R.A., and Fitzpatrick, R.W. (1990) New data and a revised structural model for ferrihydrite; discussion and reply. Clays and Clay Minerals, 38, 331–336.
Manceau, A., Gorshkov, A.I., and Drits, V.A. (1992) Structural Chemistry of Mn, Fe, Co, and Ni in Mn hydrous oxides. II. Information from EXAFS spectroscopy, electron and X-ray diffraction. American Mineralogist, 77, 1144–1157.
Manceau, A., Nagy, K.L., Spadini, L., and Ragnarsdottir, K.V. (2000) Influence of anionic layer structure of Fe-oxyhydroxides on the structure of Cd surface complexes. Journal of Colloid and Interface Science, 228, 306–316.
Manceau, A., Marcus, M.A., and Tamura, N. (2002) Quantitative speciation of heavy metals in soils and sediments by synchrotron X-ray techniques. In P. Fenter, M. Rivers, N.C. Sturchio, and S. Sutton Eds., Applications of Synchrotron Radiation in Low-Temperature Geochemistry and Environmental Science, 49, 341–428. Reviews in Mineralogy and Geochemistry, Mineralogical Society of America, Chantilly, Virginia.
Marchand, P. and Rancourt, D.G. (2009) General model for the aqueous precipitation of rough-surface nanocrystals and application to ferrihydrite genesis. American Mineralogist, 94, 1428–1439.
Marcus, M.A., Chen, H.S., and Espinosa, G.P. (1986) Distance distributions about Mn in icosahedral and crystalline AlMnSi. Solid State Communication, 58, 227–230.
Mazzetti, L. and Thistlethwaite, P.J. (2002) Raman spectra and thermal transformations of ferrihydrite and schwertmannite. Journal of Raman Spectroscopy, 33, 104–111.
Michel, F.M., Ehm, L., Antao, S.M., Lee, P.L., Chupas, P.J., Liu, G., Strongin, D.R., Schoonen, M.A.A., Phillips, B.L., and Parise, J.B. (2007) The structure of ferrihydrite, a nanocrystalline material. Science, 316, 1726–1729.
Michel, F.M., Barrónc, V., Torrent, J., Morales, M.P., Serna, C.J., Boily, J.F., Liu, Q., Ambrosini, A., Cismasu, A.C., and Brown, G.E. Jr. (2010) Ordered ferrimagnetic form of ferrihydrite reveals links among structure, composition, and magnetism. Proceedings of the National Academy of Science, 107, 2787–2792.
Mikutta, C., Mikutta, R., Bonneville, S., Wagner, F., Voegelin, A., Christl, I., and Kretzschmar, R. (2008) Synthetic coprecipitates of exopolysaccharides and ferrihydrite. Part I: Characterization. Geochimica et Cosmochimica Acta, 72, 1111–1127.
Mikutta, C., Frommer, J., Voegelin, A., Kaegi, R., and Kretzschmar, R. (2010) Effect of citrate on the local Fe coordination in ferrihydrite, arsenate binding, and ternary arsenate complex formation. Geochimica et Cosmochimica Acta, 74, 5574–5592.
O'Day, P.A., Rivera, N. Jr., Root, R., and Carroll, S.A. (2004) X-ray absorption spectroscopic study of Fe reference compounds for the analysis of natural sediments. American Mineralogist, 89, 572–585.
Ollivier, B., Retoux, R., Lacorre, P., Massiot, D., and Ferey, G. (1997) Crystal structure of kappa-alumina: An X-ray powder diffraction, TEM and NMR study. Journal of Materials Chemistry, 7, 1049–1056.
Pan, Y., Brown, A., Brydson, R., Warley, A., Li, A., and Powell, J. (2006) Electron beam damage studies of synthetic 6-line ferrihydrite and ferritin molecule cores within a human liver biopsy. Micron, 37, 403–411.
Pan, Y.H., Sader, K., Powell, J.J., Bleloch, A., Gass, M., Trinick, J., Warley, A., Li, A., Brydson, R., and Brown, A. (2009) 3D morphology of the human hepatic ferritin mineral core: New evidence for a subunit structure revealed by single particle analysis of HAADF-STEM images. Journal of Structural Biology, 166, 22–31.
Pan, Y.H., Vaughan, G., Brydson, R., Bleloch, A., Gass, M., Sader, K., Brown, A. (2010) Electron-beam-induced reduction of Fe^{3+} in iron phosphate dihydrate, ferrihydrite, haemosiderin and ferritin as revealed by electron energy-loss spectroscopy. Ultramicroscopy, 110, 1020–1032.
Pankhurst, Q.A. and Pollard, R.U. (1992) Structural and magnetic-properties of ferrihydrite. Clays and Clay Minerals, 40, 268–272.
Parise, J.B., Harrington, R., Xu, W., Michel, F.M., Hausner, D.B., Debnath, S., Strongin, D.R. (2010) Understanding the composition and structure of ferrihydrite. Geochimica et Cosmochimica Acta, 74, A793.
Patrat, G., de Bergevin, F., Pernet, M., and Joubert, J.C. (1983) Structure locale de δ-FeOOH. Acta Crystallographica, B39, 165–170.
Pauling, L. (1929) The principles determining the structure of complex ionic crystals. Journal of the American Chemical Society, 51, 1010–1026.
Post, J.E., Heaney, P.J., von Dreele, R.B., Hanson, J.C. (2003) Neutron and temperature-resolved synchrotron X-ray powder diffraction study of akaganéite. American Mineralogist, 88, 782–788.
Rancourt, D.G. and Meunier, J.F. (2008) Constraints on structural models of ferrihydrite as a nanocrystalline material. American Mineralogist, 93, 1412–1417.
Rose, J., Manceau, A., Masion, A., and Bottero, J.Y. (1997) Structure and mechanisms of formation of $FeOOH(NO_3)$ oligomers in the early stages of hydrolysis. Langmuir, 13, 3240–3246.
Saleh, A.M. and Jones, A.A. (1984) The crystallinity and surface characteristics of synthetic ferrihydrite. Clay Minerals, 19, 745–755.
Schwertmann, U. and Cornell, R.M. (1991) Iron Oxides in the Laboratory. VCH, New York.
Shinoda, K., Matsubara, E., Muramatsu, A., and Waseda, Y. (1994) Local structure of ferric hydroxide $Fe(OH)_3$ in aqueous solution by the anomalous X-ray scattering and EXAFS methods. Materials Transactions, The Japan Institute of Metals (JIM), 35, 394–398.
Shmakov, A.N., Kryukova, G.N., Tsybulya, S.V., Chuvilin, A.L., and Solovyeva, L.P. (1995) Vacancy ordering in γ-Fe_2O_3: synchrotron X-ray powder diffraction and high-resolution electron microscopy studies. Journal of Applied Crystallography, 28, 141–145.
Takagi, J., Ozaki, M., Shigemasa, K., and Mizoguchi, T. (2010) Chlorine occupancy dependence of crystal structure of pure β-phase of iron-oxyhydroxide. Materials Transactions, 51, 1330–1339.
Teo, B.K. (1986) EXAFS: basic principles and data analysis. Springer-Verlag, Berlin.
Toner, B.M., Santelli, C.M., Marcus, M.A., Wirth, R., Chan, C.S., McCollom, T. Bach, W., and Edwards, K.J. (2009) Biogenic iron oxyhydroxide formation at mid-ocean ridge hydrothermal vents: Juan de Fuca Ridge. Geochimica et Cosmochimica Acta, 73, 388–403.
Towe, K.M. and Bradley, W.F. (1967) Mineralogical constitution of colloidal "hydrous ferric oxides." Journal of Colloid and Interface Science, 24, 384–392.
Ulrich, K.U., Rossberg, A., Foerstendorf, H., Zänker, H., and Scheinost, A.C. (2006) Molecular characterization of uranium(VI) sorption complexes on iron(III)-rich acid mine water colloids. Geochimica et Cosmochimica Acta, 70, 5469–5487.
Voegelin, A., Kaegi, R., Frommer, J., Vantelon, D., and Hug, S.J. (2010) Effect of phosphate, silicate, and Ca on Fe(III)-precipitates formed in aerated Fe(II)- and As(III)-containing water studied by X-ray absorption spectroscopy. Geochimica et Cosmochimica Acta, 74, 164–186.
Waychunas, G.A., Rea, B.A., Fuller, C.C., and Davis, J.A. (1993) Surface chemistry of ferrihydrite: Part 1. EXAFS studies of the geometry of coprecipitated and adsorbed arsenate. Geochimica et Cosmochimica Acta, 57, 2251–2269.
Waychunas, G.A., Fuller, C.C., Rea, B.A., and Davis, J.A. (1996) Wide-angle X-ray scattering (WAXS) study of "two-line" ferrihydrite structure: Effect of arsenate sorption and counterion variation and comparison with EXAFS results. Geochimica et Cosmochimica Acta, 60, 1765–1781.
Xu, W., Hausner, D.B., Harrington, R., Lee, P.L., Strongin, D.R., and Parise, J.B. (2011) Structural water in ferrihydrite and constraints this provides on possible structure models. American Mineralogist, 96, 513–520.
Yamaguchi, G. and Okumiya, M. (1969) Refinement of the structure of tohdite $5Al_2O_3 \cdot H_2O$. Bulletin of the Chemical Society of Japan, 42, 2247–2249.
Yamaguchi, G., Okumiya, M., and Ono, S. (1964) The crystal structure of tohdite. Bulletin of the Chemical Society of Japan, 37, 1555–1557.
Zhukhlistov, A.P. (2001) Crystal structure of lepidocrocite FeO(OH) from the electron-diffractometry data. Crystallography Reports, 46, 730–733.

Manuscript received April 19, 2010
Manuscript accepted October 28, 2010
Manuscript handled by Barry Bickmore

Supplement for the article :

Critical evaluation of the revised akdalaite-model for ferrihydrite

A. MANCEAU

Some published TEM results supporting the standard model

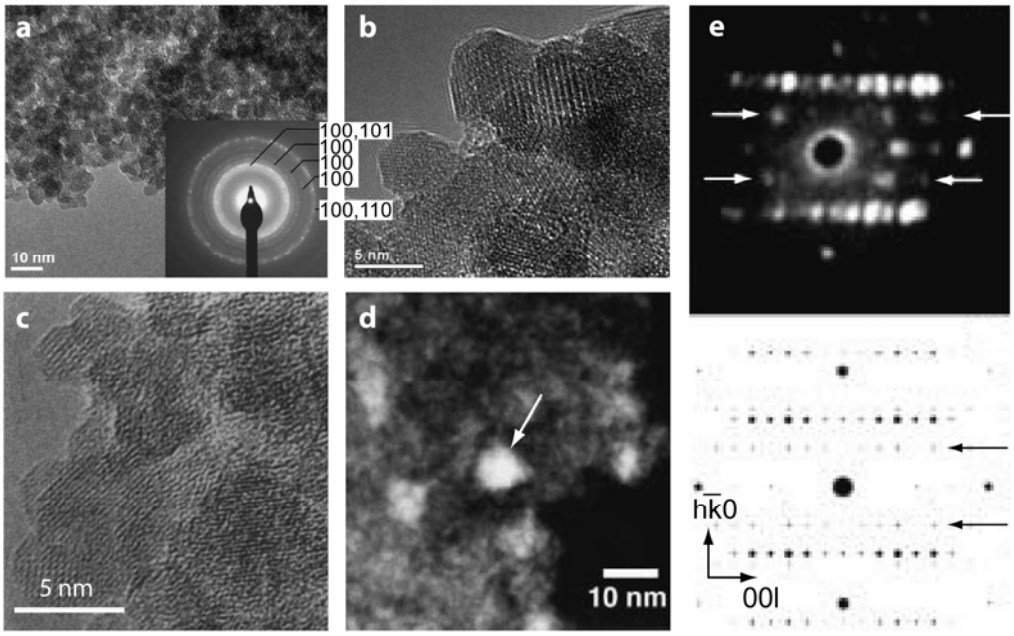

Figure S1. (a-c) Examples of HRTEM images of six-line ferrihydrite grains showing commonly observed rounded to hexagonal shapes. (d) Annular dark-field STEM images of coherently diffracting domains. The arrow points to a 10 nm single domain. (e) Nanodiffraction pattern for the [110] orientation of the f-phase with simulated pattern from the standard model. Arrows point out extra spots from the superlattice structure described by Drits et al. (1993). After Pan et al. (2006) and Janney et al. (2000, 2001).

Fe coordination from PDF and the violation of Pauling's 2nd rule

The coordination of Fe can be assessed from PDF by calculating the average Fe-O bond length because, (1), the lengths were regressed from the first PDF peak which contains all possible Fe-O correlations, (2), the presence of tetrahedral iron (^{IV}Fe) should shift this value to a shorter distance. The averages for the two successive akdalaite models are slightly different $\langle d(\text{Fe-O})_{\text{ferrifh}}\rangle$ = 2.017 Å and $\langle d(\text{Fe-O})_{\text{fhyd6}}\rangle$ = 2.00 Å, which is consistent with the fact that the PDFs were derived from different materials. The average Fe-O distance for the more recent ferrifh model matches exactly the average value of 2.015 Å for $^{VI}Fe^{3+}$ obtained from a survey of 204 Fe-O binding environments in the Inorganic Crystal Structure Database (Brown and Altermatt 1985). The average value for $^{IV}Fe^{3+}$ is shorter at 1.865 Å. If ferrihydrite contained 20% ^{IV}Fe, as in the akdalaite model, the average PDF bond length would be approximately 1.985 Å, not 2.017 Å and 2.00 Å, a difference that can be resolved by HEXS (Wells et al. 2009), especially with the precision on bond lengths of 10^{-3} Å reported by Michel et al. (2010). In addition, the higher metrical value of ferrifh suggests that the maghemite phase contained in hydromaghemite had little ^{IV}Fe, in agreement with previous studies (Liu et al. 2008; de Boer and Dekkers 2001).

The average Fe-O distance of 2.017 Å obtained by regression analysis of the PDF data for hydromaghemite (i.e., ferrifh sample) is likely correct because this value was constrained by the position of the maximum of the Fe-O correlations in the PDF. Because Michel et al. (2010) fit their data with a model structure based on that of akdalaite ($Al_{10}O_{14}(OH)_2$), which contains 20% ^{IV}Al, the optimized distribution of Fe-O distances was forced to include this coordination. In Fig. 4c of Michel et al. (2010) the calculated partial PDF for the ^{IV}Fe3 atoms has a weak peak at R ~ 1.8 Å that was attributed consistently to the ^{IV}Fe3-O4 correlation at 1.816 Å in the crystallographic model. The next peak observed at ~2.0 Å was attributed to the three O2 needed to complete the tetrahedral coordination of ^{IV}Fe3. However, this peak was listed by Michel et al. (2010) as occurring at 1.932 Å instead of ~2.0 Å (the comparable value is 2.02 Å in fhyd6). Therefore, the weak contribution of one Fe-O distance at ~1.8 Å, out of a total of 28 (Fig. 4e) in the simulation of the ferrifh PDF, is the only evidence for ^{IV}Fe. This contribution is clearly too small to be statistically significant; it was imposed by the akdalaite model to satisfy the preconceived ^{IV}Fe coordination. This is an illustration of a model-dependent optimization problem, which the PDF technique is prone to (Farrow et al. 2007; Manceau 2010).

The violation of Pauling's 2nd rule by the previous fhyd6 model was reportedly fixed in the new ferrifh model. Using the ^{IV}Fe3-O distances of 1.82 and ~2.0 Å in Figure 4c of Michel et al. (2010) and the same bond-valence method as the authors (Brown and Altermatt 1985), ^{IV}Fe3 receives approximately 0.85 + 0.52 x 3 = 2.41 v.u. from the O4 and three O2 oxygens, not 2.74 as misrepresented in their Table S4. The valence sum problem does not seem to have been completely solved by the ferrifh model, which appears to violate both Pauling's 2nd and distortion rules.

Lastly, Xu et al. (2011) observed by PDF that the first shell Fe-O distance decreases from 1.99 Å to 1.96 Å when ferrihydrite is transformed to hematite upon heating. This reduction of the average Fe-O distance with temperature is a strong argument against the presence of tetrahedral Fe in ferrihydrite. If Fh contained 20% ^{IV}Fe as in the akdalaite-like model, then the average Fe-O bond length could only increase with temperature because hematite has only octahedral Fe. A tetrahedron is smaller than an octahedron, therefore a reduction of distance is inconsistent with a coordination change from tetrahedral to octahedral.

EXAFS data of akaganeite at room and liquid nitrogen temperatures

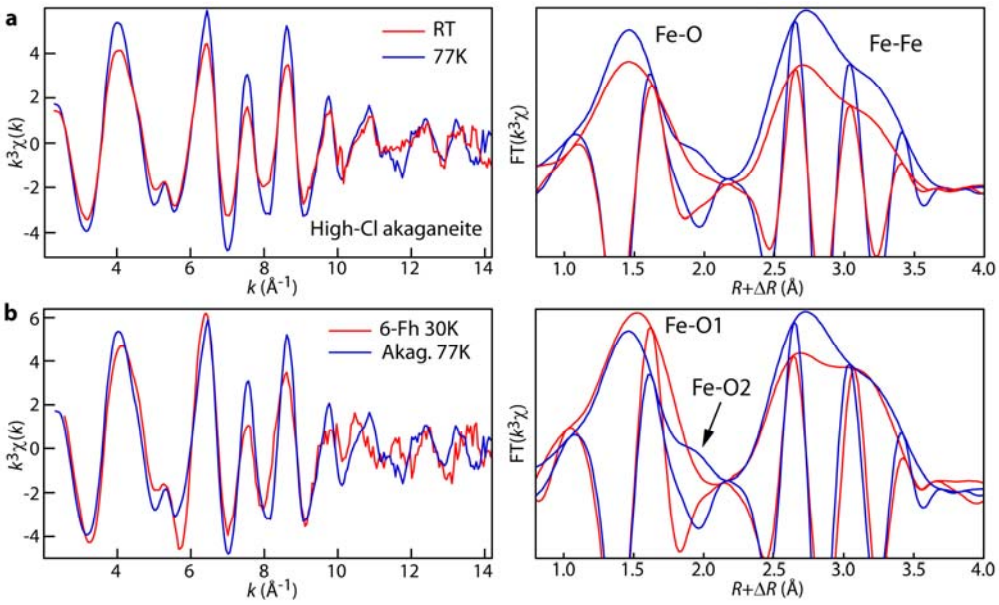

Figure S2. EXAFS (left) and Fourier transforms (right) for high-Cl akaganeite at room and liquid nitrogen temperatures (a), and for high-Cl akaganeite at 77K and six-line ferrihydrite at 30K (b). Akaganeite was prepared by neutralizing to neutral pH a 0.1 M $FeCl_3$ solution.

Lowering the temperature increases the sensitivity of EXAFS to the long Fe-O distances at 2.10-2.20 Å in both akaganeite and ferrihydrite. Ferrihydrite has a mean Fe-O1 distance of R =1.98 Å (after correction of the ΔR phase shift) and akaganeite R = 1.95 Å (Table 1). A distance of 1.98 Å for 6Fh is the value usually reported in the literature. The difference to the nominal 2.01 Å value for ^{VI}Fe does not mean that ferrihydrite contains ^{IV}Fe, but that EXAFS analysis from room temperature data excludes the full distribution of interatomic distances.

Multiple versus single shell EXAFS analysis

The contributions to EXAFS of the Fe-O and Fe-Fe pairs were fit simultaneously in k space with WinXAS v. 3.2 (Ressler, 1998). Theoretical backscattering phases and amplitudes were calculated with FEFF v. 7 (Ankudinov and Rehr 1997) using goethite as structural model (Hazemann et al. 1991). The $R + \Delta R$ window of the Fourier backtransforms varied from 0.9-3.5 Å to 0.9-3.7 Å. The procedure used to calculate the confidence limits for CN_j, R_j and σ_j reported in Table S1 is described in Ressler et al. (2010).

Caution is advocated to not analyze separately the anionic (O) and cationic (Fe) shells in k space, in particular the Fe-O pair because its contribution partly overlaps with the most intense Fe-Fe wave function. The importance of truncation errors introduced by a shell-by-shell analysis of ferrihydrite is evaluated below with the theoretical spectrum of goethite (Fig. 3 of Manceau 2009), and with the experimental data of feroxyhite and 6Fh. Fitting a model spectrum (i.e., goethite) provides unambiguous information about the reliability of the EXAFS data-analysis procedure.

Truncation effects on data itself caused by the finite data range and overlapping shells is illustrated in Figure S3a with the single scattering $\chi_{Fe\text{-}O}$ function of goethite, (1), calculated directly with FEFF, and (2), Fourier-filtered from the total *ab initio* EXAFS spectrum. The two functions are clearly not the same, showing distinct differences in shape and wave frequency at several k values. In agreement with theory, the least-squares fit spectrum is superpimposed on the unfiltered $\chi_{Fe\text{-}O}$ function, and the regressed parameters are identical to crystallographic values used to calculate $\chi_{Fe\text{-}O}$ (Fig. S3b). When the analysis is performed on the Fourier filtered function, the best-fit parameters are in close proximity to crystallographic values only if the two Debye-Waller terms (σ_{O1} and σ_{O2}) or coordination numbers (CN_{O1} and CN_{O2}) are constrained to the same value during minimization (Fig. S3c). Otherwise, if $\sigma_{O1} \neq \sigma_{O2}$ and $CN_{O1} \neq CN_{O2}$, then R_{O1} and R_{O2} decrease by 0.03-0.04 Å and the fit is improved due to the higher number of degrees of freedom in the regression (Fig. S3d).

The influence of the Fourier transform truncation on the fit variances of feroxyhite and 6Fh are shown in Figure S4. Results show that truncation effects are even more important in disordered materials. In both cases, an unrealistic distance of 1.87 Å is obtained when neither σ nor CN are constrained, and statistical tests show considerable covariance of some fit parameters.

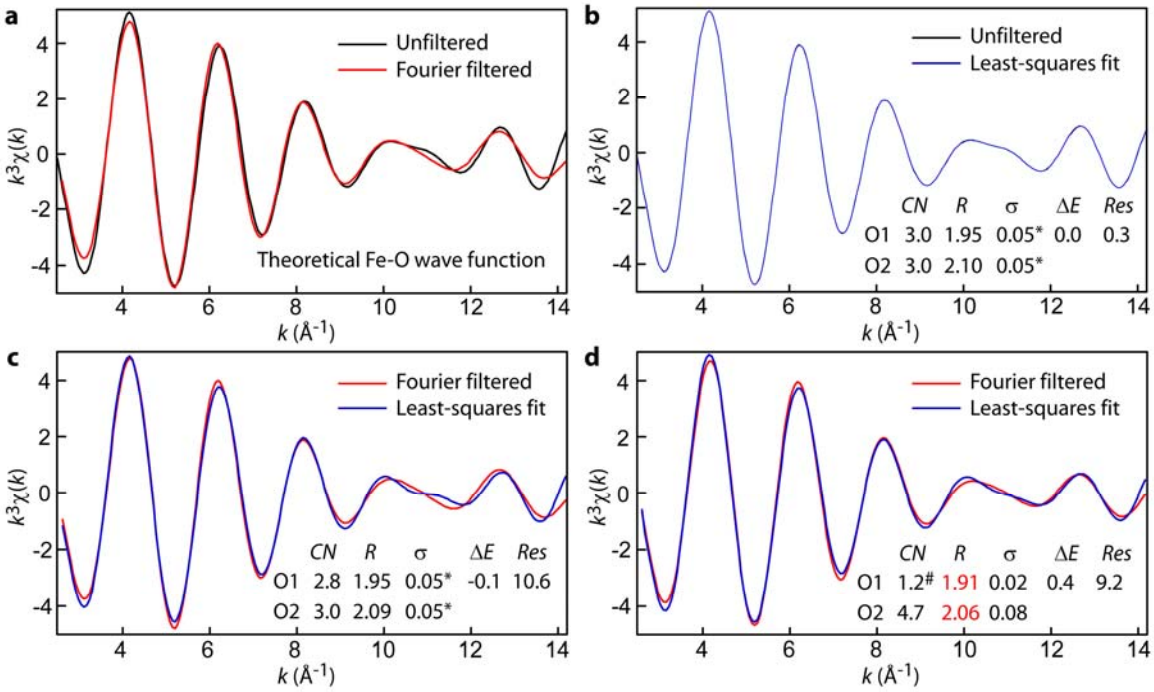

Figure S3. (a) Theoretical $\chi_{Fe\text{-}O}$ wave function for goethite calculated with FEFF v. 7 (unfiltered) and Fourier-filtered from the total *ab initio* EXAFS spectrum. The theoretical electronic wave was calculated using the following crystallographic values for the first atomic shell: R_{O1} = 1.95 Å, R_{O2} = 2.10 Å, σ = 0.005 Å. Additional details can be found in Manceau (2009). (b-d) Least-squares fits and best-fit values of the unfiltered and Fourier-filtered $\chi_{Fe\text{-}O}$ functions. When σ_{O1} and σ_{O2} are optimized independently (d), several parameters are strongly correlated and the minimization algorithm converges to a local minimum with short Fe-O distances. #: fixed value to prevent divergence of σ_{O1} to negative values.

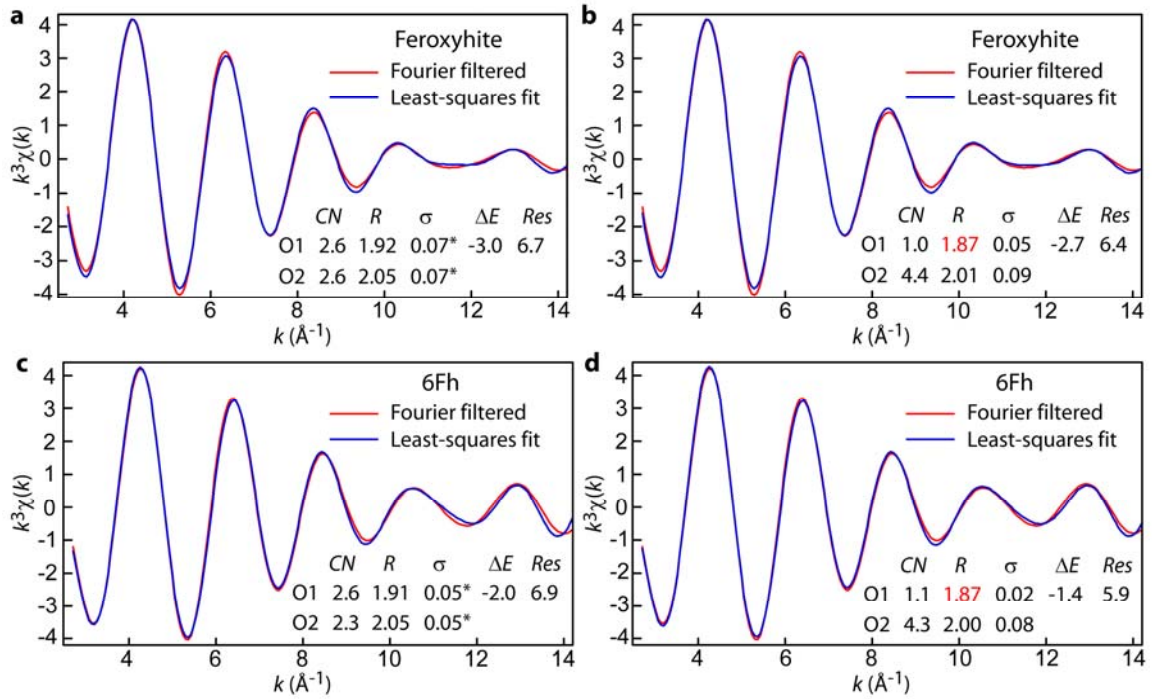

Figure S4. Single-shell fits of the Fourier filtered $\chi_{Fe\text{-}O}$ function for feroxyhite and 6Fh. When σ_{O1} and σ_{O2} are optimized independently (b,d), the fit converges to R_{O1} = 1.87 Å and CN_{O1} exhibits a F-test value of 0.9 and the error exceeds its best-fit value (precision > 100%).

References

Ankudinov, A.L. and Rehr, J.J. (1997) Relativistic calculations of spin-dependent X-ray-absorption spectra. Physical Review, B56, 1712-1716

Brown, I.D. and Altermatt, D. (1985) Bond-valence parameters obtained from a systematic analysis of the Inorganic Crystal Structure Database. Acta Crystallographica, B41, 244-247.

De Boer, C.B. and Dekkers, M.J. (2001) Unusual thermomagnetic behaviour of haematites: neoformation of a highly magnetic spinel phase on heating in air. Geophysical Journal International, 144, 481-494.

Drits, V.A., Sakharov, B.A., Salyn, A.L., and Manceau, A. (1993) Structural model for ferrihydrite. Clay Minerals, 28, 185-208.

Farrow, C.L., Juhas, P., Liu, J.W., Bryndin, D., Bozin, E.S., Bloch, J., Proffen, T., and Billinge S.J.L. (2007) PDFfit2 and PDFgui: computer programs for studying nanostructure in crystals. Journal of Physics: Condensed Matter, 19, 335219.

Janney, D.E., Cowley, J.M., and Buseck, P.R. (2000) Transmission electron microscopy of synthetic 2- and 6-line ferrihydrite. Clays and Clay Minerals, 48, 111-119.

Janney, D.E., Cowley, J.M., and Buseck P.R. (2001) Structure of synthetic 6-line ferrihydrite by electron nanodiffraction. American Mineralogist, 86, 327-335.

Liu, Q., Barron, V., Torrent, J., Eeckhout, S.G., Deng, C. (2008) Magnetism of intermediate hydromaghemite in the transformation of 2-line ferrihydrite into hematite and its paleoenvironmental implications. Journal of Geophysical Research, 113, 1-12.

Manceau, A (2009) Evaluation of the structural model for ferrihydrite derived from real-space modeling of high-energy X-ray diffraction data. Clay Minerals, 44, 19-34.

Manceau, A. (2010) PDF analysis of ferrihydrite and the violation of Pauling's Principia. Clay Minerals, 45, 225-228.

Michel, F.M., Barrónc, V., Torrent, J., Morales, M.P., Serna, C.J., Boily, J.F., Liu, Q., Ambrosini, A., Cismasu, A.C., and Brown Jr. G.E. (2010) Ordered ferrimagnetic form of ferrihydrite reveals links among structure, composition, and magnetism. Proceedings of the National Academy of Science of the United States of America, 107, 2787-2792.

Pan, Y., Brown, A., Brydson, R., Warley, A., Li, A., and Powell, J. (2006) Electron beam damage studies of synthetic 6-line ferrihydrite and ferritin molecule cores within a human liver biopsy. Micron, 37, 403-411.

Ressler, T. (1998) WinXAS: a program for X-ray absorption spectroscopy data analysis under MS-Windows. Journal of Synchrotron Radiation, 5, 118-122.

Ressler, T., Walter, A., Scholz, J., Tessonnier, J.P., and Su, D.S. (2010) Structure and properties of a Mo oxide catalyst supported on hollow carbon nanofibers in selective propene oxidation. Journal of Catalysis, 271, 305–314.

Wells, D.M., Jin, G.B., Skanthakumar, S., Haire, R.G., Soderholm, L., Ibers, J.A. (2009) Quaternary neptunium compounds: Syntheses and characterization of $KCuNpS_3$, $RbCuNpS_3$, $CsCuNpS_3$, $KAgNpS_3$, and $CsAgNpS_3$. Inorganic Chemistry, 48, 11513-11517.

Zhu W., Hausner D.B., Harrington R., Lee P.L., Strongin D.R., Parise J.B. (2011) Structural water in ferrihydrite and constraints this provides on possible structure models. American Mineralogist, DOI: 10.2138/am.2011.3460

Table S1. Confidence limits of the fitting parameters calculated from a variation of the residual (*Res*) within 90% of its optimal value

	Fe-O1			Fe-O2			Fe-Fe1			Fe-Fe2/Fe3		
	Δ*CN*	Δ*R* (Å)	Δσ (Å)	Δ*CN*	Δ*R* (Å)	Δσ (Å)	Δ*CN*	Δ*R* (Å)	Δσ (Å)	Δ*CN*	Δ*R* (Å)	Δσ (Å)
Feroxyhite – 3rd model-fit	-	0.01	-	0.1	0.01	0.03	0.7(0.62)	0.01	-	1.0(0.80)	0.01	-
										0.8(0.70)	0.02	0.01
6Fh - 1st strategy	-	0.01	0.03(0.46)	0.1	0.01	0.04(0.50)	1.0(0.70)	0.02	-	1.3(0.79)	0.01	0.02
- 2nd strategy	-	0.01	0.03(0.48)	0.1	0.01	0.04(0.43)	1.3(0.73)	0.02	0.07(0.53)	1.1(0.72)	0.01	0.05(0.61)
6-Fh 30K – 2nd model-fit	0.3	0.01	-	0.3(0.55)	0.05(0.68)	0.02	1.0(0.74)	0.01	0.05(0.58)	0.5(0.66)	0.008	0.04(0.63)
High-Cl akaganeite 77K	-	0.014	0.04(0.76)	0.2	0.023	0.06(0.54)	0.5(0.48)	0.01	-	0.6(0.57)	0. 04	-
										0.9(0.67)	0.02	0.02

In parenthesis are correlations from the F-test. Parameters with $0.5 < F < 0.8$ are moderately correlated and those with $0.8 < F < 1.0$ are highly. Correlated values have higher standard deviations.